Article

Cell Chemical Biology

Clionamines stimulate autophagy, inhibit *Mycobacterium tuberculosis* survival in macrophages, and target Pik1

Graphical abstract

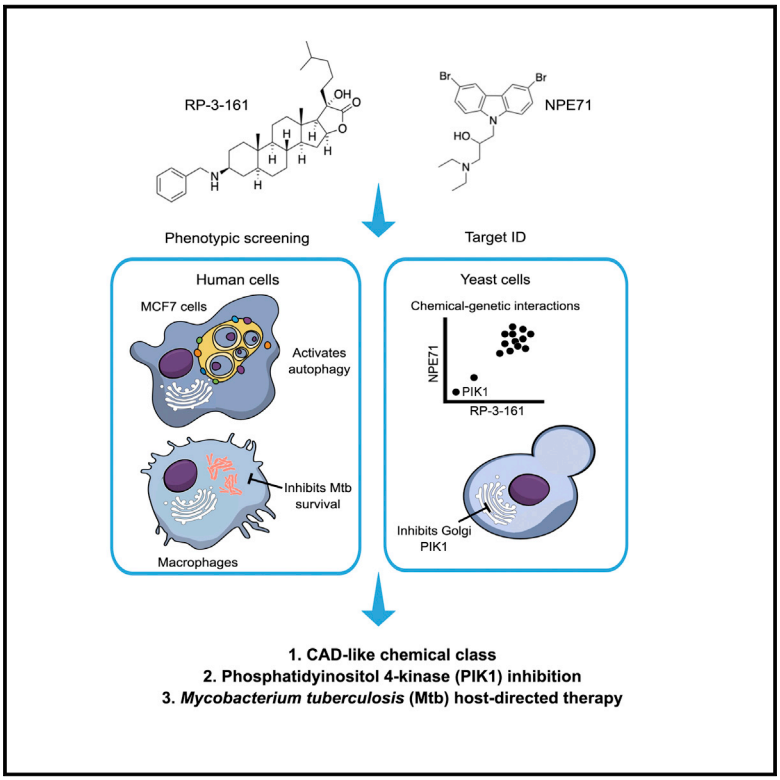

Highlights

- Clionamines activate autophagy and inhibit Mtb survival in macrophages
- Yeast chemical genetics identified Pik1 as a clionamine target protein
- SiRNA knockdown of PI4KB inhibited the survival of Mtb in macrophages
- PI4KB has been identified as an unexploited target for drugs to treat tuberculosis

Authors

Rosanne Persaud, Sheena C. Li, Joseph D. Chao, ..., Yossef Av-Gay, Michel Roberge, Raymond J. Andersen

Correspondence

charlie.boone@utoronto.ca (C.B.), yossi@mail.ubc.ca (Y.A.-G.), michelr@mail.ubc.ca (M.R.), raymond.andersen@ubc.ca (R.J.A.)

In brief

Persaud et al. have shown that the sponge natural product clionamines activate autophagy, inhibit Mtb in macrophages, and target the PI4 kinase Pik1 in yeast. siRNA knockdown of PI4KB, a human homolog of Pik1, inhibited Mtb survival in macrophages, identifying PI4KB as an unexploited target for HDT drugs to treat tuberculosis.

Persaud et al., 2022, Cell Chemical Biology *29*, 870–882
May 19, 2022
https://doi.org/10.1016/j.chembiol.2021.07.017

CellPress

CellPress

Cell Chemical Biology

Article

Clionamines stimulate autophagy, inhibit *Mycobacterium tuberculosis* survival in macrophages, and target Pik1

Rosanne Persaud,[1,9] Sheena C. Li,[5,7,9] Joseph D. Chao,[3,9] Roberto Forestieri,[1] Elizabeth Donohue,[2] Aruna D. Balgi,[2] Xingji Zheng,[3] Jesse T. Chao,[4] Yoko Yashiroda,[7] Mami Yoshimura,[7] Christopher J.R. Loewen,[4] Anne-Claude Gingras,[8] Charles Boone,[5,6,7,*] Yossef Av-Gay,[3,*] Michel Roberge,[2,*] and Raymond J. Andersen[1,10,*]

[1]Departments of Chemistry and Earth Ocean & Atmospheric Sciences, University of British Columbia, 2036 Main Mall, Vancouver, BC V6T 1Z1, Canada

[2]Deptartment of Biochemistry and Molecular Biology, University of British Columbia, 2350 Health Sciences Mall, Vancouver, BC V6T 1Z3, Canada

[3]Division of Infectious Disease, Departments of Medicine and Microbiology and immunology, University of British Columbia, 2350 Health Sciences Mall, Vancouver, BC V6T 1Z3, Canada

[4]Department of Cellular and Physiological Sciences, University of British Columbia, 2350 Health Sciences Mall, Vancouver, BC V6T 1Z3, Canada

[5]Donnelly Centre for Cellular and Biomolecular Research, University of Toronto, 160 College Street, Toronto, ON M5S 3E1, Canada

[6]Department of Molecular Genetics, University of Toronto, 160 College Street, Toronto, ON M5S 3E1, Canada

[7]RIKEN Center for Sustainable Resource Science, 2-1 Hirosawa, Wako, Saitama, Japan

[8]Lunenfeld-Tanenbaum Research Institute at Mount Sinai Hospital, 600 University Avenue, Toronto, ON M5G 1X5, Canada

[9]These authors contributed equally

[10]Lead contact

*Correspondence: charlie.boone@utoronto.ca (C.B.), yossi@mail.ubc.ca (Y.A.-G.), michelr@mail.ubc.ca (M.R.), raymond.andersen@ubc.ca (R.J.A.)

https://doi.org/10.1016/j.chembiol.2021.07.017

SUMMARY

The pathogen *Mycobacterium tuberculosis* (Mtb) evades the innate immune system by interfering with autophagy and phagosomal maturation in macrophages, and, as a result, small molecule stimulation of autophagy represents a host-directed therapeutics (HDTs) approach for treatment of tuberculosis (TB). Here we show the marine natural product clionamines activate autophagy and inhibit Mtb survival in macrophages. A yeast chemical-genetics approach identified Pik1 as target protein of the clionamines. Biotinylated clionamine B pulled down Pik1 from yeast cell lysates and a clionamine analog inhibited phosphatidyl 4-phosphate (PI4P) production in yeast Golgi membranes. Chemical-genetic profiles of clionamines and cationic amphiphilic drugs (CADs) are closely related, linking the clionamine mode of action to co-localization with PI4P in a vesicular compartment. Small interfering RNA (siRNA) knockdown of PI4KB, a human homolog of Pik1, inhibited the survival of Mtb in macrophages, identifying PI4KB as an unexploited molecular target for efforts to develop HDT drugs for treatment of TB.

INTRODUCTION

Tuberculosis (TB) resulting from infection with *Mycobacterium tuberculosis* (Mtb) is the world's leading cause of death from an infectious bacterial disease (World Health Organization, 2020). The World Health Organization reported that in 2018 there were an estimated 10 million new TB cases diagnosed and 1.5 million TB deaths worldwide, along with a significant increase in reported cases of multidrug-resistant TB (MDR-TB). Most people infected with Mtb initially develop asymptomatic infection (latent TB), which can emerge many years later and progress to an active disease state, often with a lethal outcome (Chee et al., 2018). There is an urgent need to find new approaches to treating MDR-TB and latent TB infections that are not responsive to current antimycobacterial chemotherapy treatment regimens (Young et al., 2020; Dheda et al., 2017). Development of host-directed therapeutics (HDT) aimed at activating the xenophagy (selective autophagy) component of the innate immune system represents a promising approach to providing drugs to counter the dual threat of MDR and latent TB infections (Gupta et al., 2016; Zumla et al., 2016; Kim et al., 2019; Kimmey and Stallings, 2016; Kaufmann et al., 2018; Wallis and Hafner, 2015; Paik et al., 2019; Sharma et al., 2018; Machelart et al., 2017).

The primary site of Mtb infections are the circulating alveolar macrophage cells. This route of infection exposes Mtb to xenophagy, the selective autophagy mechanism that human cells utilize to destroy invading viral and bacterial pathogens (Levine et al., 2011; Kim et al., 2019; Kimmey and Stallings, 2016). To counter this threat, Mtb has developed ways to thwart xenophagy,

allowing it to reside and multiply inside macrophages. Xenophagy in Mtb-infected macrophages starts with formation of an isolation membrane that elongates to a phagophore used to capture the Mtb bacterial cargo (Lamb et al., 2013). The phagophore subsequently grows and matures into an autophagosome that completely engulfs an Mtb cell before fusing with a lysosome to access the enzymes used to degrade and kill the captured cells. Yeast genomic studies have shown that at least 35 autophagy-related (Atg) genes are involved in the regulation of the complex biology of canonical and selective autophagy (Mizushima et al., 2011).

The processes of inhibiting phagocytosis/autophagy/xenophagy and the maturation of autophagosomes by Mtb effectors is well studied. We have shown that an Mtb-secreted tyrosine phosphatase PtpA inhibits the phagosome-lysosome fusion by dephosphorylating vacuolar protein sorting 33B (VPS33B), which is the regulator of membrane fusion (Bach et al., 2008). PtpA also alters the V-ATPase machinery on the phagosome, preventing its maturation (Wong et al., 2011). Others have shown that the Enhanced Intracellular Survival (EIS) protein of Mtb inhibits autophagy by mediating the AKT/mTOR pathway via activation of IL-10 (Duan et al., 2016).

A phosphatidylinositol 3-kinase (PI3K) complex consisting of Atg14L, BECLIN1, VPS15, and the kinase VPS34 produces phosphatidylinositol 3-phosphate (PI3P) in the phagophore, which is essential for maturation of the phagophore into an autophagosome in xenophagy (Fratti et al., 2001). Mtb cells captured in the macrophage phagophore release a glycosylated phosphatidylinositol (mannose-capped lipoarabinomannan [LAM]) to inhibit PI3P formation by the kinase VPS34 (Kang et al., 2005; Fratti et al., 2003; Vergne et al., 2003) and the PI3P phosphatase SapM (Saleh and Belisle, 2000; Vergne et al., 2005) to remove any residual PI3P that escapes the LAM inhibition of VPS34 (Deretic et al., 2006). This highly effective two-pronged approach to removing PI3P from the macrophage Mtb phagosome prevents its maturation into an autophagosome, allowing Mtb to escape xenophagy destruction and colonize the macrophages, supporting its pathogenicity.

The increase in our understanding of how Mtb evades the innate immune system by blocking xenophagy has prompted researchers to explore the potential of overcoming the immune block via small molecule stimulation of autophagy as a standalone or adjunct HDT approach to treatment of TB infections. A common feature of many of these studies has been the evaluation of known drugs that could be repurposed as autophagy activators. An important study showed that the mechanism of action of the frontline TB drugs isoniazid and pyrazinamide involved both direct antimycobacterial activity and autophagy stimulation (Kim et al., 2012). We found that the antiprotozoal drug nitazoxanide also inhibited Mtb survival in human macrophage THP-1 cells by combined antimycobacterial and autophagy-stimulating effects (Lam et al., 2012; NIH, 2016). Other examples of compounds able to inhibit the survival of Mtb in macrophages via autophagy stimulation include the antidiarrheal drug loperamide (Juarez et al., 2016); the antidepressant drug fluoxetine (Stanley et al., 2014); the anti-leukemia drug ibrutinib (Hu et al., 2020); the expectorant ambroxol, used in the treatment of respiratory diseases (Choi et al., 2018); the SMERS (Small Molecule Enhancers of Rapamycin) 10, 18, and 28 (Floto et al., 2007); the herbal medicine baicalin (Zhang et al., 2017); and the plant natural product pasakbumin A (Lee et al., 2019).

As part of a program designed to find marine natural product modulators of autophagy and identify their protein targets, we discovered that clionamines A (**1**) and B (**2**) (Figure 1) isolated from the South African sponge *Cliona celata* were effective stimulators of autophagy and autophagic flux in human breast cancer MCF7 cells (Keyzers et al., 2008). The potential of autophagy-stimulating compounds to reduce survival of Mtb in macrophages as described above prompted us to investigate the ability of the clionamines to inhibit Mtb survival in THP-1 macrophages. Since the amount of natural clionamines available for these studies was very small, a synthesis of clionamine B (**2**) was undertaken in order to provide sufficient material for further biological evaluation (Forestieiri et al., 2013). Described below are the details of a structure activity relationship (SAR) analysis of the autophagy-activating properties of synthetic clionamine analogs; the effectiveness of clionamines at inhibiting Mtb survival in THP-1 macrophages; the identification of a cellular target of the most effective autophagy-stimulating synthetic analog RP-3-161 (**5**) and the natural product clionamine B; the relationship of the bioactivity profile of the clionamines to NPE71, a compound with cationic amphiphilic drug (CAD) characteristics; and a small interfering RNA (siRNA) knockdown study of the putative clionamine target in macrophages.

RESULTS

Inhibition of Mtb survival in THP-1 macrophages by clionamines A (1) and B (2)

Prior to the synthesis of clionamine analogs, we examined the ability of the autophagy-activating natural product clionamine A (**1**) and synthetic clionamine B (**2**) (Forestieiri et al., 2013) to inhibit the survival of Mtb in macrophages. The assay uses an Mtb H37Rv strain expressing a luciferase reporter gene. Luminescence produced upon addition of luciferin is an indication of the total amount of luciferase expressed by the Mtb and can be used as an indication of the metabolic status of the Mtb inside the cell. Clionamine A (**1**) and clionamine B (**2**) both inhibited Mtb survival in human macrophages at single-digit micromolar concentrations (Figure 2) (MIC_{50}s [minimum inhibitory concentrations required to inhibit the growth of 50% of organisms]) clionamine A [**1**] $\approx$ 7 μM; clionamine B [**2**] $\approx$ 8 μM) that were in the same concentration range that stimulated autophagy in human MCF-7 breast cancer cells (Keyzers et al., 2008; Forestieiri et al., 2013). Neither clionamine A nor B showed significant cytotoxicity to THP-1 macrophages at their MIC_{50}s.

Synthesis of clionamine analogs for SAR analysis

Before starting on an extensive SAR study, we first prepared *N*-acetyl clionamine (**3**) and 3-aminochloestane (**4**) (Figure 1) to explore the requirement for a C-3 primary amine and the E ring α-hydroxy-γ-lactone substructures of clionamine A (**1**) for autophagy activation. Neither **3** nor **4** showed any autophagy activation in the MCF-7 cell-based screening assay, suggesting that both the C-3 primary amine functionality and the E ring γ-lactone moieties are required parts of the clionamine autophagy-activating pharmacophore and, therefore, that there was a reasonable probability of clionamines binding to a unique protein molecular target.

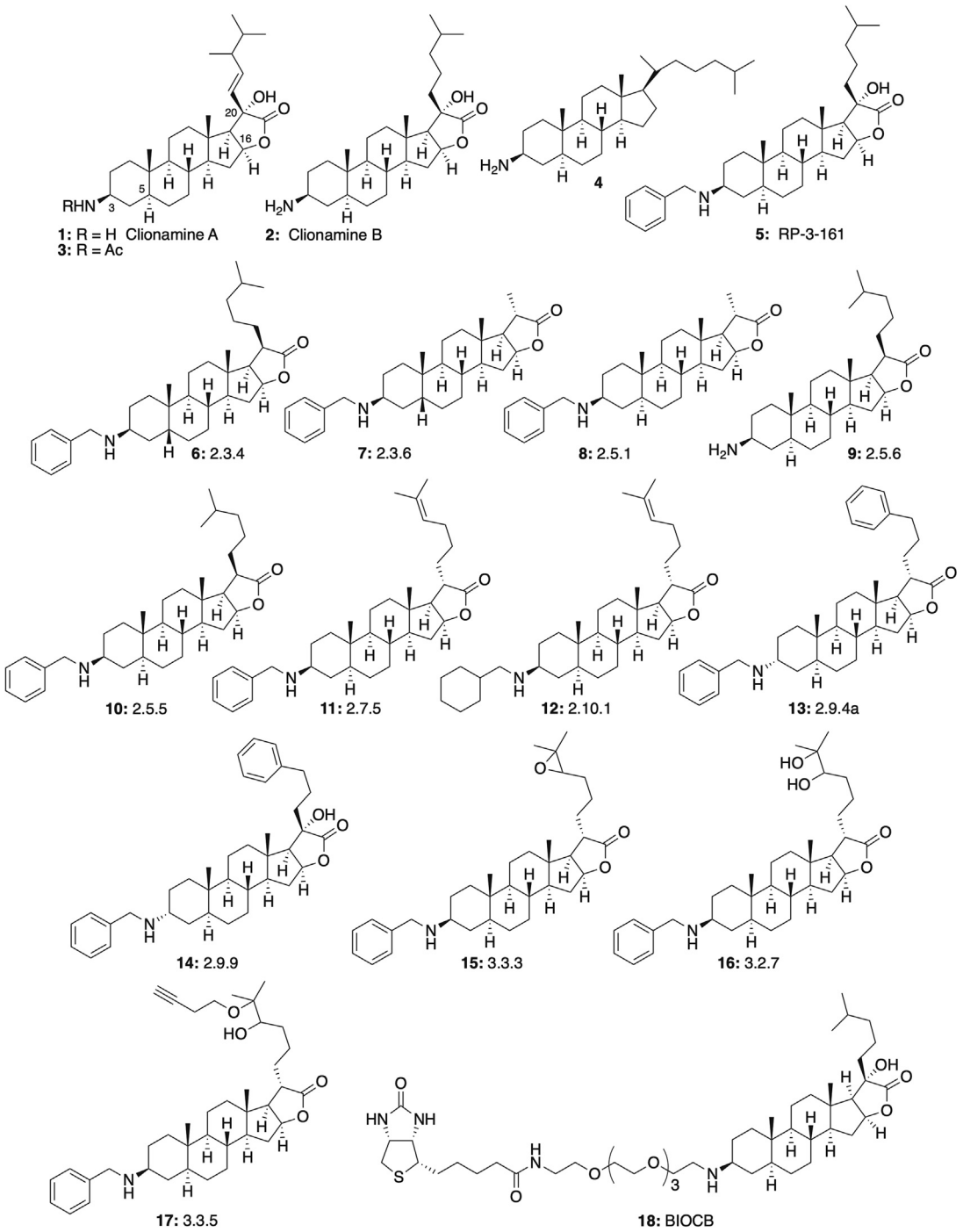

Figure 1. Marine natural product clionamines and a library of synthetic clionamine analogs

The goal of the analog study was to explore the role of the various substructures in the clionamine autophagy-stimulating pharmacophore with the aim of generating an analog that was synthetically accessible in quantities required for additional biological evaluation and ideally more potent and/or efficacious than the natural products clionamine A (**1**) and B (**2**). Toward this end, we examined the effect of scaffold changes at the C-3 primary amine, the C-5 configuration, the C-20 hydroxyl, and the C-20 alkyl side chain substituents. Making the analogs required an efficient synthetic route. Our published synthesis of clionamine B (**2**) (Forestieiri et al., 2013) provided a flexible route to making the desired scaffold analogs and a subsequent report of the synthesis of clionamine D (Wang et al., 2014) revealed a more efficient methodology for constructing a key α-methylene lactone intermediate. Our optimized second-generation synthetic route to clionamine B (**2**) (Scheme S1)

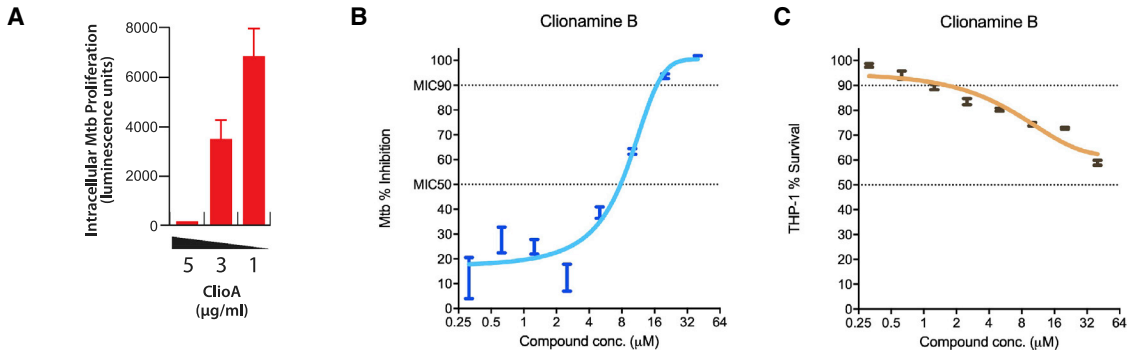

Figure 2. Natural clionamine A (1) [ClioA] and synthetic clionamine B (2) inhibit survival of Mtb in human THP-1 macrophages

The intracellular survival of Mtb was measured using a luciferase assay. Data were normalized using DMSO as a negative control, corresponding to 100% bacterial growth, and 20 μM rifampicin as a positive control, corresponding to 100% inhibition of bacterial growth. THP-1 survival was measured using an MTT assay. Data were normalized to DMSO as a negative control corresponding to 100% THP-1 survival and represent the mean ± SEM. Non-linear regression was used to fit the data of the log (inhibitor) versus response (variable slope) curve using GraphPad Prism analysis software.

(A) Clionamine A (**1**) inhibition of Mtb in THP-1 macrophages. (3 mg/mL = 6.7 mM), n = 3.

(B) Clionamine B (**2**) inhibition of Mtb in THP-1 macrophages, n = 3.

(C) THP-1 survival when treated with clionamine B (**2**), n = 3.

combines elements of both published syntheses of clionamines. The small library of clionamine analogs shown in Figure 1 was prepared by making minor modifications to the optimized synthetic route to clionamine B (**2**).

Autophagy activation assays

The synthetic analogs **5** to **17** shown in Figure 1 along with the natural product clionamine A (**1**) were tested for their ability to activate autophagy in a cell-based assay designed to detect modulators of autophagosome accumulation. This assay uses human breast cancer MCF7 cells transfected with a plasmid for expressing GFP-LC3 (Green Fluorescent Protein-Light Chain 3) (Balgi et al., 2009). LC3 is known to be recruited to the membranes of autophagosomes when autophagy is stimulated. Therefore, a positive indication of autophagy stimulation is the appearance of green fluorescent dots (puncta) upon incubating cells expressing the autophagic marker GFP-LC3 for a period of time with a small molecule compound. Quantification of the degree of stimulation of autophagy is carried out using fluorescence microscopy to measure punctate GFP-LC3 fluorescence.

Compounds were tested in two batches (see Figures S1 and S2 in supplemental information) based on the time period separating the preparation of the first group of analogs **5** to **14**, and the second group of analogs **15** to **17**. The most potent analog RP-3-161 (**5**) from the first batch was used as a positive control in the second batch to capture the relative potencies of the first group and the second group. Five of the analogs, 2.5.4 (**5**), 2.3.4 (**6**), 2.3.6 (**7**), 2.5.1 (**8**), and 2.5.5 (**10**), showed strong punctate fluorescence accumulation at 10 μg/mL (Figures S1 and S2). Analogs 2.5.6 (**9**), 2.7.5 (**11**), 2.10.1 (**12**), 2.9.4a (**13**), 3.3.3 (**15**), 3.2.7 (**16**), and 3.3.5 (**17**), and as well as clionamine A (**1**), showed relatively little punctate fluorescence accumulation in comparison with the five active compounds. The punctate fluorescence accumulation data at 10 μg/mL revealed that either β or α C-5 configuration gave strong activity (i.e., 2.3.4 [**6**] and 2.5.5 [**10**]; 2.3.6 [**7**], and 2.5.1 [**8**]), that the C-21 OH was not essential for strong activity (i.e., 2.5.4 [**5**] versus 2.5.5 [**10**]), and that a short methyl side chain, even in the α configuration, was sufficient for strong activity (i.e., 2.3.6 [**7**] and 2.5.1 [**8**]). It was also clear that a C-3 benzyl amine, as found in all of the strongly active analogs (2.5.4 [**5**], 2.3.4 [**6**], 2.3.6 [**7**], 2.5.1 [**8**], and 2.5.5 [**10**]), was superior to a C-3 free amine (2.5.6 [**9**] and clionamine A [**1**]). Interestingly, the relatively inactive analogs 2.7.5 (**11**), 2.10.1 (**12**), 2.9.4a (**13**), 3.3.3 (**15**), 3.2.7 (**16**), and 3.3.5 (**17**) all have the unnatural C-20 α side chain configuration, which may be the detrimental factor. A C-20 methyl side chain in the α configuration in the strongly active compounds 2.3.6 (**7**) and 2.5.1 (**8**) is presumably too small to generate the negative steric interaction responsible for the relative inactivity observed for analogs with larger C-20 side chains in the α configuration. The data (Figure S1) show that RP-3-161 (2.5.4 [**5**]) gave a clear dose-response curve in the concentration range of 1–10 μg/mL, gave the strongest response of all of the analogs at 3 μg/mL, and was more efficacious than clionamine A (**1**) at all concentrations.

Several of the potent (2.5.4 [**5**], 2.3.4 [**6**], 2.3.6 [**7**], 2.5.5 [**10**]) and weakly active (2.7.5 [**11**], 2.10.1 [**12**]) analogs identified from the data were next evaluated for their ability to generate autophagic flux. Autophagic flux refers to the entire process of autophagy, which includes autophagosome formation, maturation, fusion with lysosomes, and subsequent breakdown and release of macromolecules back into the cytosol. When autophagic flux is increased by an autophagy stimulator, the LC3 segment of GFP-LC3 is degraded, but the GFP portion is more resistant to proteolysis and appears as a lower-molecular-weight band. Figure 3A shows that the positive control rapamycin and RP-3-161 (2.5.4 [**5**]) show similar significant autophagic flux consistent with autophagy stimulation, while the other analogs that were tested showed minimal or no autophagic flux at 10 μg/mL.

RP-3-161 (5) inhibition of intracellular survival of Mtb in human macrophage

Aside from inducing autophagic flux, RP-3-161 (2.5.4 [**5**]) also inhibits Mtb survival in THP-1 macrophage cells (Figure 3B) with an

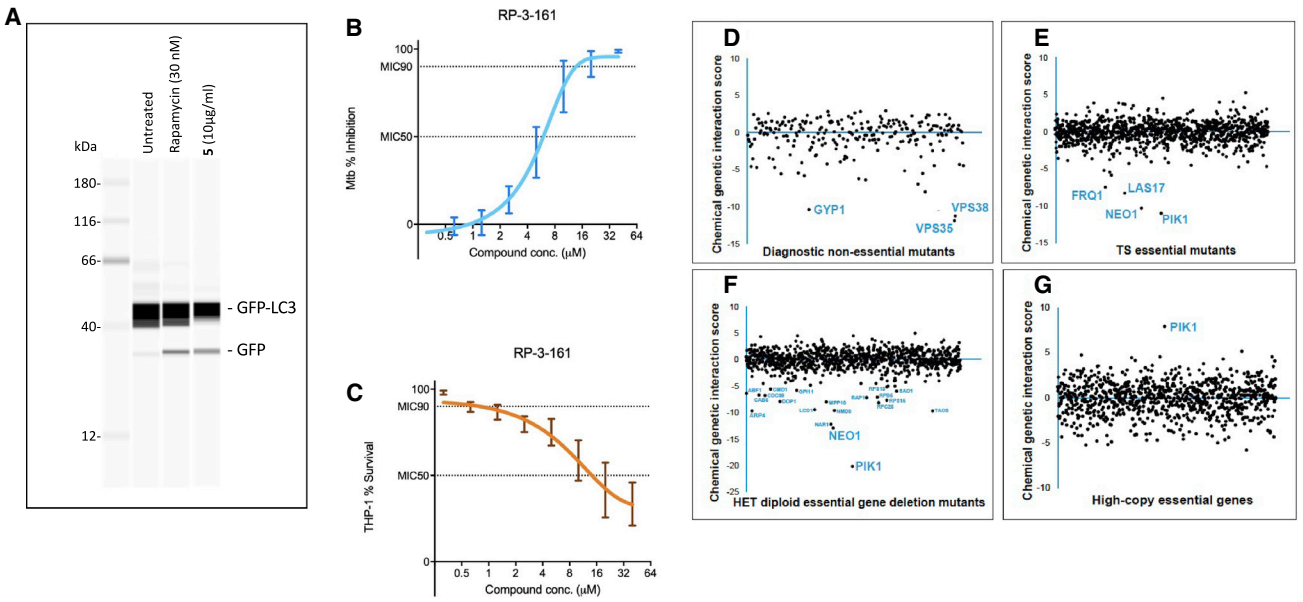

Figure 3. Biological activities of RP-3-161 (5)

(A) Automated capillary electrophoresis western analysis showing stimulation of autophagic flux in MCF7 human breast cancer cells by the synthetic clionamine analog RP-3-161 (**5**). Rapamycin was used as a positive control. The molecular weight marker lane is shown at the left.

(B) Dose-response curve of RP-3.161 (**5**). THP-1 cells infected with Mtb expressing the luciferase gene were treated with increasing concentrations of RP-3-161 (**5**), Data represent the mean ± SEM, n = 4. Non-linear regression was used to fit the data of the log (inhibitor) versus response (variable slope) curve using GraphPad Prism analysis software.

(C) THP-1 survival was measured using an MTT assay. Data represent the mean ± SEM ,n = 6. Non-linear regression was similarly used to fit the data as above.

(D–G) Predicting the targets of RP-3-161 using chemical genomics. Chemical genetic profiles for RP-3-161 were obtained using several *S. cerevisiae* mutant libraries. The relative abundances of each mutant were quantified after pooled growth in the presence of various compound concentrations. Profiles at concentrations that showed the best separation between outlier chemical genetic interactions and the mean *Z* score for all interactions in the profile were selected. (D) A diagnostic set profile from a library of 310 non-essential gene deletion mutants that are representative of major biological functions was obtained at 1 μg/mL. (E) A TS mutant profile from a library of 1,181 temperature-sensitive mutants for yeast genes that are essential for viability was obtained at a screening concentration of 3 μg/mL (IC22). (F) A HET mutant profile from a library of 968 HET diploid mutants for essential genes was obtained at screening concentration of 10 μg/mL (IC76). (G) A MoBY overexpression profile from a library of 960 strains that overexpress essential genes was obtained at a screening concentration of 2 μg/mL (IC93).

MIC_{50} (≈6–8 μM) comparable with clionamines A (**1**) and B (**2**) (Figure 2), showing that RP-3-161 is a potent analog that has anti-Mtb and autophagy-stimulating activities similar to the original natural product clionamines.

Identification of RP-3-161's (5) cellular target using yeast haploinsufficiency screening

RP-3-161 (2.5.4 [**5**]) was the most effective synthetic analog stimulator of MCF-7 GFP-LC3 punctate fluorescence accumulation at 3 and 10 μg/mL (Figures S1 and S2, supplemental information), it produced significant autophagic flux in the western blot assay (Figure 3A), and it inhibited survival of Mtb in THP-1 macrophages with an MIC_{50} comparable with clionamines A and B (Figure 3B). Therefore, based on all of the data in hand, RP-3-161 (2.5.4 [**5**]) was selected as a tool compound to facilitate identification of the protein molecular target(s) associated with clionamine stimulation of autophagy and xenophagic inhibition of Mtb survival in THP-1 macrophages.

RP-3-161 (**5**) inhibits the growth of *Saccharomyces cerevisiae*, suggesting it may target a highly conserved protein or pathway. To explore the yeast pathways that are particularly important for cell fitness in the presence of RP-3-161, we employed a high-throughput chemical-genetic platform. RP-3-161 was screened against several genome-wide, DNA-barcoded *S. cerevisiae* mutant collections, which enable quantification of the relative abundance of each mutant after compound treatment via barcode sequencing. The set of yeast non-essential genes was analyzed with a relatively small number of diagnostic deletion gene mutants covering 310 functionally diverse genes (Piotrowski et al., 2017). The set of ~1,000 yeast essential genes was analyzed with three different strain collections, each of which spanned the majority of essential genes, including a set of temperature-sensitive (TS) mutants (Li et al., 2011), a set of heterozygous (HET) diploid deletion mutants (Lee et al., 2014), and a set of yeast strains each carrying an essential gene on a high-copy plasmid (Ho et al., 2009). Because *S. cerevisiae* has highly efficient pleiotropic drug efflux systems, each of the four mutant collections was constructed in a drug-hypersensitive genetic background (*pdr1Δpdr3Δsnq2Δ*) (Piotrowski et al., 2017). The mutant collections were grown in a pooled competitive growth assay in the presence of RP-3-161. Following outgrowth of each pool, the relative abundance of individual mutants was assessed through next-generation sequencing of strain barcodes.

The diagnostic non-essential gene deletion mutant chemical-genetic profile of RP-3-161 identified three highly sensitive genes, *VPS35*, *VPS38*, and *GYP1* (Figure 3D), all of which are involved in vesicle transport (Kihara et al., 2001; Robinson et al., 1988; Seaman et al., 1998). *VPS35* encodes an endosomal

subunit of the membrane-associated retromer complex that is required for retrograde transport (Seaman et al., 1997), *VPS38* codes for a component of the phosphatidylinositol 3-kinase complex (Burda et al., 2002; Kihara et al., 2001), and *GYP1* encodes a cis-Golgi GTPase-activating protein for yeast Rab proteins that plays a role in vesicle docking and fusion, and interacts with autophagosome component Atg8 (Du and Novick, 2001; Mitter et al., 2019). Because genes that are functionally related to the mode of action of RP-3-161 are expected to show chemical-genetic interactions with RP-3-161 (Parsons et al., 2004), these findings suggest that RP-3-161 may target a pathway involved in vesicle trafficking.

The most sensitive mutant in the essential TS mutant chemical-genetic profile of RP-3-161 carried a mutation in *PIK1* (Figure 3E), which encodes a phosphatidylinositol 4-kinase that catalyzes the first step in the biosynthesis of the Golgi pool of phosphatidylinositol-4-phosphate (PI4P) (Flanagan et al., 1993; Seaman et al., 1998). Another highly sensitive mutant carried a TS allele of *FRQ1*, which encodes an intracellular signaling protein that activates the Pik1 enzyme (Hendricks et al., 1999; Huttner et al., 2003). RP-3-161-sensitive TS mutants also included *NEO1*, which encodes a Golgi-localized phospholipid flippase that establishes phospholipid asymmetry of the plasma membrane and is involved in vesicle-mediated transport (Hua and Graham, 2003; Takar et al., 2016; Wicky et al., 2004), and *LAS17*, which encodes a member of the WASP protein family that is involved in nucleation of branched actin filaments that drive endocytosis in yeast (Li, 1997; Madania et al., 1999; Urbanek et al., 2013). *PIK1* and *FRQ1* are the most highly sensitive genes, suggesting that RP-3-161 may modulate phosphatidylinositol-4-phosphate biosynthesis or a pathway whose function is dependent on PI4P.

The HET diploid deletion mutant collection is particularly powerful because a given mutant may be reduced for an essential gene product by ~50%, thereby rendering HET mutant cells sensitive to compounds targeting the deleted gene (Costanzo et al., 2010; Giaever et al., 1999; Lee et al., 2014). We found that the *pik1/PIK1* HET diploid was the most hypersensitive to RP-3-161 (Figure 3F), suggesting that the Pik1 protein may be a direct target of RP-3-161. Alternatively, RP-3-161 may modulate another gene product or pathway that depends on normal levels of PI4P.

The essential gene, high-copy plasmid strain collection provides a way of increasing potential target gene dosage, which should lead to a resistance phenotype in the presence of a compound that specifically inhibits the target gene product (Ho et al., 2009). From an unbiased screen, we identified the *PIK1* overexpression strain as the most resistant to RP-3-161 (Figure 3G) at the highest concentration of the compound tested (2 μg/mL, IC94), which further implicates Pik1 as a potential target for RP-3-161.

We also generated chemical-genetic profiles for clionamine B and found interactions with similar genes (Figure S3). Clionamine B was screened against all non-essential deletion mutants to provide a higher-resolution profile than the diagnostic set (Figure S3A). Like RP-3-161, clionamine B had a chemical-genetic interaction with *GYP1*, the Golgi GTPase-activating protein that interacts with autophagosome protein Atg8. Moreover, the TS, HET, and molecular barcoded yeast (MoBY) profiles for clionamine B consistently had interactions with *NEO1* and *PIK1* mutants (Figures S3B–S3D). The highly similar chemical-genetic interactions of clionamine B and RP-3-161 confirmed that RP-3-161 was a reasonable tool compound for elucidating the molecular target of the natural product clionamines.

RP-3-161 (5) inhibits the yeast PI4 kinase *in vivo* at the trans-Golgi network

We next tested the ability of RP-3-161 to inhibit Pik1 at the TGN. Using wild-type yeast cells, we first observed a dose-dependent inhibition of growth (Figure 4). Specifically, at 80 μg/mL, RP-3-161 caused a 3-fold increase in doubling time (Figure 4B). Since PI4P is essential for growth in yeast, this suggested that RP-3-161 could abolish PI4P synthesis in a concentration-dependent manner. To investigate whether RP-3-161 (**5**) specifically inhibited Pik1 at the trans-Golgi network (TGN), we used a PI4P-specific fluorescent probe, GFP-Osh2-PH (Shin et al., 2020). In wild-type yeast cells under normal growth conditions, GFP-Osh2-PH localized mostly to the TGN, with a minor fraction localizing to the plasma membrane, consistent with the known distribution of intracellular PI4P (Bennett et al., 2006) (Figure 4C, first row). In contrast, a higher concentration of RP-3-161 (80 μg/mL) led to an immediate decrease in TGN-localized PI4P; after 1 h, almost all PI4P was re-localized to the plasma membrane (Figure 4C, second row). Expectedly, a lower concentration of RP-3-161 (50 μg/mL) resulted in a smaller fraction of GFP-Osh2-PH showing a redistribution, but a similar effect was still evident (Figure 4C, third row). Finally, upon shifting a TS conditional mutant of *PIK1*, *pik1-104*, to a non-permissive temperature, we observed an effect that was similar to that of RP-3-161 with almost no PI4P at the TGN (Figure 4C, fourth row). Quantifications of peak GFP-Osh2-PH fluorescence intensity at the TGN clearly showed that RP-3-161 exposure resulted in loss of PI4P after 1 h (Figure 4D). All in all, we concluded that RP-3-161 specifically inhibited Pik1-dependent synthesis of PI4P in the TGN.

Pik1 interacts with biotinylated clionamine B

We synthesized a biotinylated clionamine B probe BIOCB (**18**), which is also a close analog of RP-3-161 (**5**) (supplemental information, Scheme S1), and performed affinity purification coupled to mass spectrometry (AP-MS) from a wild-type *S. cerevisiae* strain as well as a strain that overexpressed *PIK1*, and compared the BIOCB (**18**) physical interactions with those recovered on biotin-cholesterol. To identify significant interactions with our compound, statistical analysis of four replicate purifications from probe BIOCB (**18**) against streptavidin beads alone and streptavidin beads bound to biotin-cholesterol was performed using SAINTexpress (Teo et al., 2014). Proteins with false discovery rates equal to or below 1% were classified as statistically significant clionamine interactors. The alpha and beta subunits of fatty acid synthetase, Fas2p and Fas1p, were precipitated from yeast lysates using biotinylated cholesterol (Table S2). In lysates from a PIK1-overproducing strain, Pik1 precipitated with both BIOCB (**18**) and biotinylated cholesterol, but we observed a 7-fold stronger effect with probe BIOCB (**18**) and Pik1, suggesting that clionamines form a more specific interaction with Pik1 (Figure 5A and Table S2). Dop1 and Mon2 were also identified as significant clionamine-specific interacting proteins in the same AP-MS assay (Figure 5A and Table S2). Dop1 and Mon2 control the activation of Neo1 (Dalton et al., 2017), which functions as a

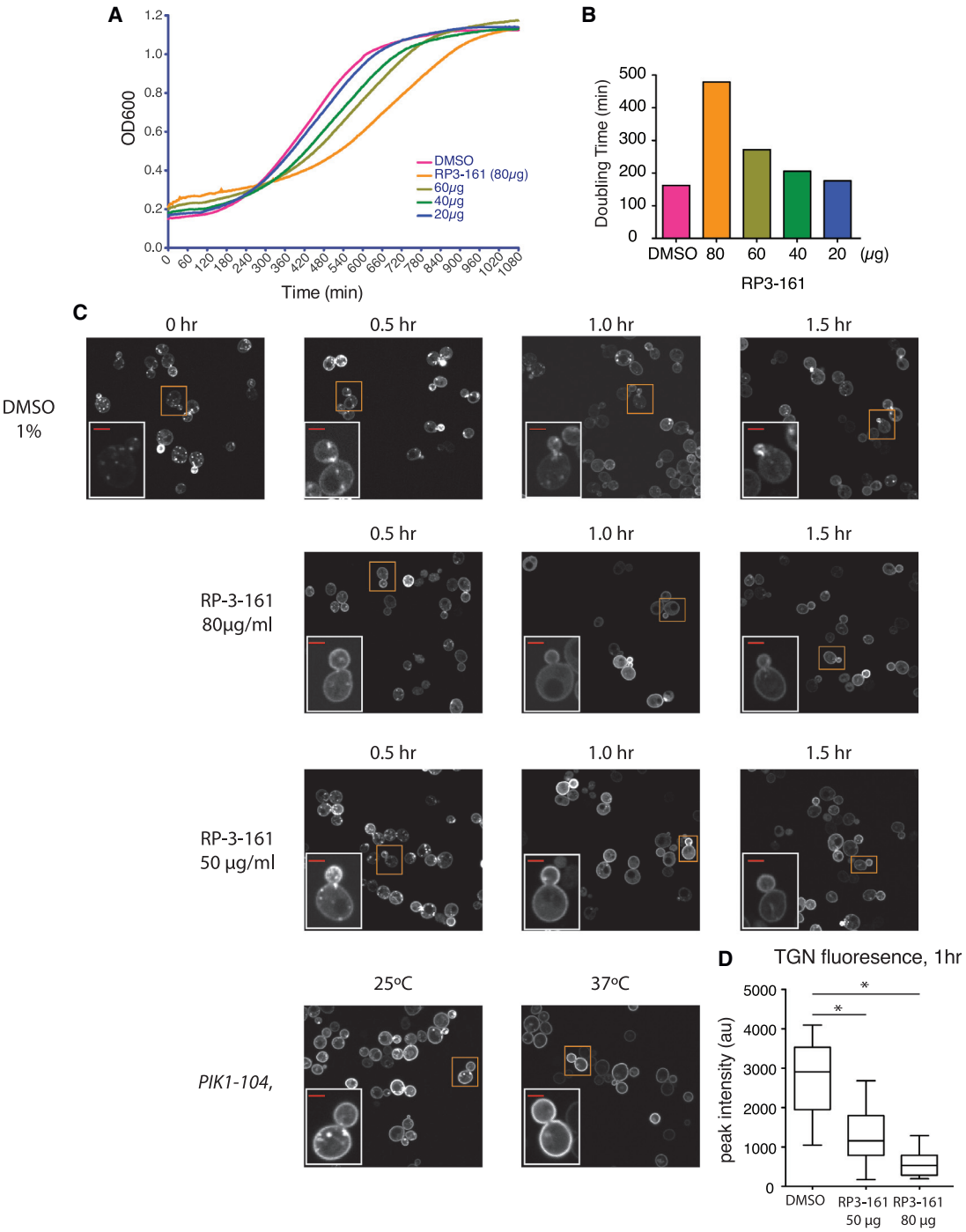

Figure 4. RP-3-161 inhibits the yeast PI4 kinase *in vivo* at the TGN

(A) Growth curve analysis of wild-type yeast grown in synthetic complete (SC) medium supplemented with DMSO or RP-3-161 at μg/mL concentrations indicated in (A) and (B).

(B) Doubling times calculated from the growth curves in (A).

(C) Confocal images of yeast cells expressing GFP-Osh2-PH from a plasmid taken at the indicated time points. Wild-type cells were grown in SC medium with either DMSO or RP-3-161 at indicated concentrations. *PIK1-104* cells were grown initially at 25°C, then incubated at the non-permissive temperature (37°C) for 1 h. All scale bars, 2 μm.

(D) Quantifications of GFP-Osh2-PH localized to the TGN. *p < 0.0001.

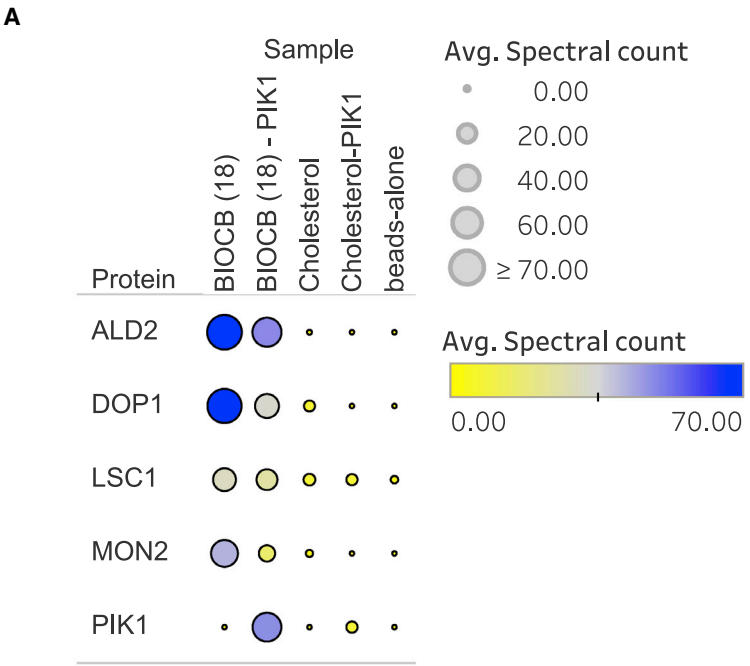

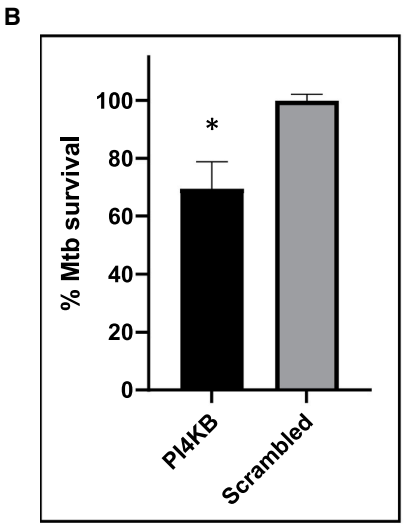

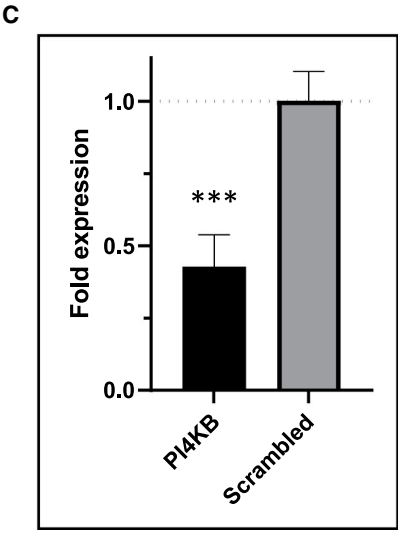

Figure 5. Overproduced PIK1 interacts with biotinylated clionamine B, and siRNA knockdown of PI4KB inhibits Mtb survival in macrophages

(A) Interaction between biotinylated clionamine B and PIK1

Proteins that most strongly interact with biotinylated clionamine B were determined by AP-MS from a wild-type *S. cerevisiae* strain (BIOCB (**18**), n = 3, SAINT false discovery rate ≤1%) as well as a strain that overproduced *PIK1* (BIOCB (**18**)-PIK1). The mean spectral count for each interacting protein is represented by circle size and color scale. Samples that were loaded with biotinylated cholesterol and beads alone served as controls. The clionamine B-PIK1 interaction is only observed using cell lysate extracted from a *PIK1*-overproducing yeast strain, but is 7-fold stronger than the cholesterol-PIK1 interaction from the same overproducing strain (BIOCB (**18**)-PIK1, n = 1; cholesterol-PIK1, n = 2).

(B) Inhibition of intracellular Mtb by siRNA-knockdown of PI4KB. Differentiated THP-1 cells were transfected with PI4KB or scrambled siRNA followed by infection with RFP-expressing Mtb. Rifampicin-treated cells were used as a positive control for 100% killing. The percentage Mtb survival was calculated as a percentage of the fluorescence from the scrambled siRNA control after subtracting average fluorescence of the rifampicin control (background) and represent the mean ± SEM, n = 4. Statistics were performed using a two-tailed t test compared with the scrambled siRNA control. p = 0.0179.

(C) siRNA knockdown efficiency. Quantitative real-time PCR comparing PI4KB mRNA levels in THP-1 cells transfected with PI4KB siRNA or scrambled siRNA. Average of six biological samples performed in quadruplicate ± SEM, n = 4. p = 0.0002 using a two-tailed Welch's t test.

phospholipid flippase that translocates phosphatidylserine (PS) and phosphatidylethanolamine (PE) from the exoplasmic to the cytoplasmic leaflet of membrane bilayers and thereby establishes an asymmetric distribution of these lipids (Takar et al., 2019). Notably, compounds that have a *pik1/PIK1* HET chemical-genetic interaction also frequently have HET chemical-genetic interactions with *NEO1* (Lee et al., 2014).

Comparison of RP-3-161 with other CAD-like compounds

NEO1-PIK1 HET chemical-genetic interactions are a hallmark "signature" of CADs, which are associated with drug-induced phospholipidosis, a human phospholipid storage disorder. The *NEO1-PIK1* chemical-genetic signature is thought to arise from the accumulation of CADs in acidic vacuolar and lysosomal compartments, preventing the proper function of Neo1 and Pik1 (Lee et al., 2014). Indeed, we found that the CAD-like compounds NPE71 (**19**) (Figure 6) and clionamine B (**2**) (supplemental information, Figure S3) showed chemical-genetic interactions that were highly similar to that of RP-3-161 (**5**) with all of our strain collections, namely the non-essential deletion gene mutants, TS, HET, and MoBY strains (Figure 4) (Piotrowski et al., 2017). Moreover, NPE71 led to reduced TGN localization of our GFP-Osh2-PH reporter, suggesting that NPE71 inhibits Pik1 in yeast cells (Figure S4) like RP-3-161 (Figure 4). Thus, RP-3-161 targets Pik1 in yeast cells and this activity is likely linked to its CAD-like properties and its concentration in a Pik1-localized compartment.

Several known drugs, such as the antidepressant fluoxetine, that stimulate autophagy and inhibit Mtb survival in macrophages (Stanley et al., 2014) have typical CAD-like structures. We have shown that fluoxetine has a strong *NEO1-PIK1* chemical-genetic interaction signature similar to RP-3-161, NPE71, and clionamine B, suggesting that it may also be modulating PI4Ks (Figure S5).

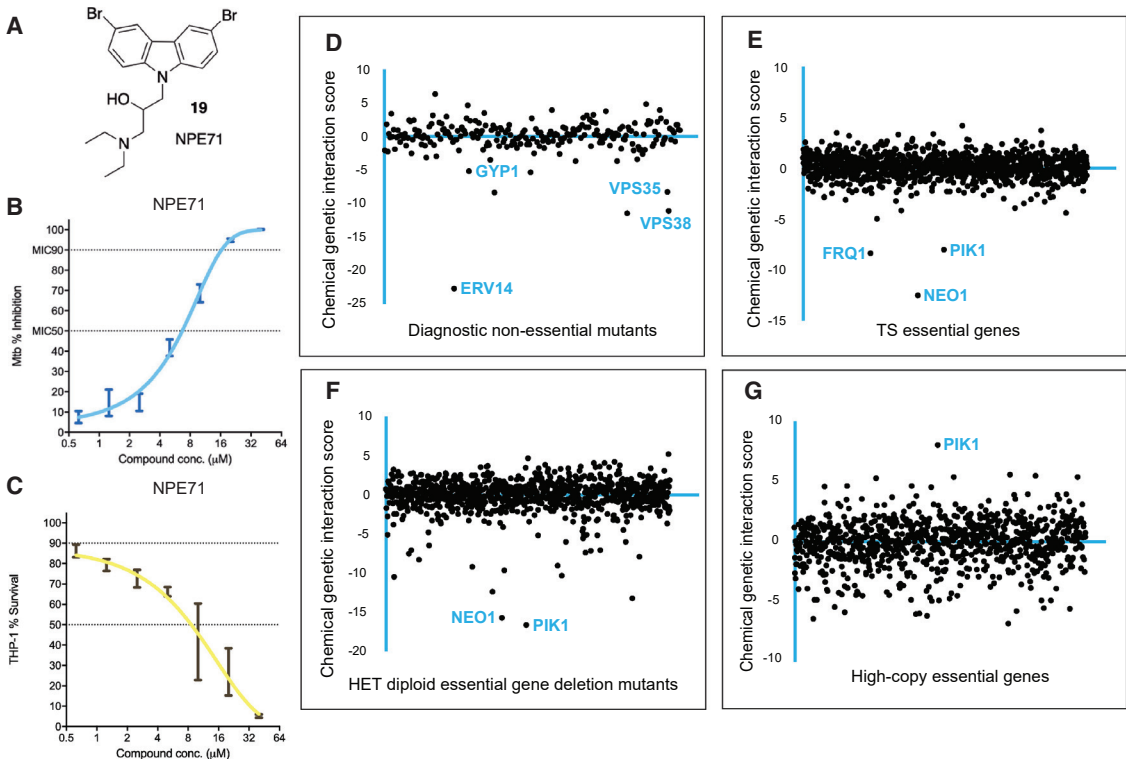

Figure 6. NPE71 (19), a CAD-like compound, shares a common *NEO1-PIK1* HET chemical-genetic signature with RP-3-161, and also inhibits the survival of Mtb in macrophages

(A) Chemical structure of the CAD compound NPE71 (**19**).

(B) NPE71 (**19**) inhibits survival of Mtb in human THP-1 macrophages. Data represent the mean ± SEM, n = 3. Non-linear regression was used to fit the data of the log (inhibitor) versus response (variable slope) curve using GraphPad Prism analysis software.

(C) THP-1 survival when treated with NPE71, measured using an MTT assay. Data represent the mean ± SEM, n = 3. Non-linear regression was similarly used to fit the data as above.

(D) A diagnostic set profile was obtained at a screening concentration of 0.5 μg/mL.

(E) A TS mutant profile was obtained at a screening concentration of 5 μg/mL (IC5).

(F) A HET mutant profile was obtained at a screening concentration of 5 μg/mL (IC67).

(G) A MoBY overexpression profile was obtained at a screening concentration of 4 μg/mL (IC91).

siRNA knockdown of PI4KB impairs Mtb survival in macrophages

In order to test whether the RP-3-161 inhibition of PI4KB, the human homolog of Pik1, affects Mtb survival in infected macrophages (THP-1), we tested whether siRNA knockdown of PI4KB could mimic compound inhibition. As seen in Figure 5B, siRNA interference in PI4KB expression resulted in impaired Mtb survival in THP-1 cells compared with cells treated with scrambled siRNA. Transcription analysis using quantitative real-time PCR showed incomplete, yet significant, siRNA knockdown of PI4KB (Figure 5C), and thus may explain the partial inhibition (≈30%) of Mtb intracellular growth. These results validate PI4KB as a viable cellular target for HDTs against Mtb worthwhile of further investigation.

DISCUSSION

Natural products have historically been an excellent source of life-saving antibiotics that target microbial pathogens directly. There is an urgent ongoing need for new drugs to treat Mtb infections, and natural products continue to represent one of the richest sources of novel antimicrobial drug lead scaffolds. In addition to providing chemical inspiration for the development of new antibacterial therapies, knowledge of the molecular target of any new natural product drug lead has become an expected requirement for serious consideration as a clinical candidate (Williams and Andersen, 2020). Recently there has been a growing interest in trying to circumvent antibiotic drug resistance by developing host-directed therapies that target human cells. Several frontline drugs used to treat tuberculosis activate autophagy and this property is thought to play a role in their clinical effectiveness (Kim et al., 2012).

We found that the marine natural product clionamines (A [**1**] and B [**2**]) effectively stimulate autophagy in MCF7 cells (Keyzers et al., 2008; Forestieiri et al., 2013) and inhibit the survival of Mtb in THP-1 macrophages. An optimized total synthesis of clionamine B (**2**) has been developed that provided an effective route for making analogs used for SAR analysis of chemical moieties that were important parts of the clionamine autophagy-stimulating pharmacophore. We found that the configuration at C-5 of the steroid AB ring junction did not seem to be important for

autophagy stimulation, suggesting that the A ring end of the compound is not directly binding a protein target. On the other hand, the configuration of C-20, the attachment point for the steroid side chains, is critical. All of the active compounds (at 10 μg/mL) with a side chain larger than a single methyl group have the C-20 β configuration, while analogs with the C-20 α configuration are only weakly active. A C-3 benzyl amine substituent was present in all of the strongly active compounds but not in the weakly active compounds. The C-20 hydroxyl was not essential for activity, but RP-3-161 (**5**), the most potent and efficacious autophagy stimulator, has the C-20 α OH.

To identify the molecular target of RP-3-161 (**5**), we employed a high-throughput chemical-genetic platform in *S. cerevisiae*, which measured the effect of compound exposure on the fitness of hundreds of mutants defective for functionally diverse genes that span the entire yeast genome. We linked the activity of RP-3-161 to the vesicular trafficking pathway, and specifically to *PIK1*, which encodes the yeast phosphatidylinositol-4-kinase (PI4K), which maintains the Golgi pool of PI4P, and *NEO1*, which encodes a Golgi-localized phospholipid flippase. Combining information from various types of chemical-genetic mutant screens suggested that RP-3-161 may directly target Pik1, or it may modulate another protein or pathway that depends on normal PI4P levels. Since *NEO1* and PIK1 HET diploid chemical-genetic interactions represent a commonly found signature in chemical-genetic screens for compounds with cationic and amphiphilic properties (CADs), we studied the physiological effect of another CAD-like molecule, NPE71, in our autophagy and Mtb survival assay. While NPE71 exposure did not generate autophagic flux at the concentration tested (10 μg/mL), we did observe that NPE71 treatment led to inhibition of Mtb survival in THP-1 macrophages. Interestingly, we found that RP-3-161 inhibits the yeast PI4 kinase *in vivo*, since compound exposure led to decreased levels of TGN-localized PI4P, and NPE71 treatment led to a similar reduction in trans-Golgi PI4P levels. Pik1 was detected with biotinylated clionamine B in a streptavidin-mediated pulldown assay in cells overexpressing *PIK1*, as well as Dop1 and Mon2, which form a complex with Neo1 and control its activity (Dalton et al., 2017). The streptavidin pulldown probe had the biotin attached at the A ring amine, leaving the E ring lactone and C-20 side chains of the steroid exposed for binding. Combining this information with the autophagy SAR analyses suggests a specific clionamine binding interaction occurring via the E ring lactone end of the molecule. Moreover, all the strongly active compounds in the autophagy SAR assay had a benzyl substituent on the C-3 amine. It is possible that this lipophilic structural feature points to the importance of the CAD-like physical properties of the active compounds, where lipophilicity around the basic nitrogen is important for activity. In summary, these results suggest that the anti-Mtb properties of RP-3-161, clionamine B, and NPE71 in macrophages are due to their activity against PI4K. This mode of action is linked to their CAD-like properties and co-localization with PI4P in a vesicular compartment. We have also shown that the CAD-like antidepressant drug fluoxetine, which has been reported to activate autophagy and inhibit Mtb in macrophages, has the *NEO1-PIK1* chemical-genetic interaction signature exhibited by RP-3-161, NPE71, and clionamine B, suggesting that the PI4K inhibitory HDT activity against Mtb may be widely shared by CADs.

Finally, siRNA knockdown of PI4KB, the human homolog of PIK1, led to inhibition of Mtb survival in THP-1 macrophages, validating PI4KB as a viable host-directed therapy cellular target against Mtb. Phosphatidylinositols have been implicated in the regulation of autophagy (O'Farrell et al., 2013). PI3P has been reported to activate autophagy and phosphatidylinositol 3,4,5-triphosphate (PI(3,4,5)P3) has been reported to be a block or brake on autophagy. A potential role for PI4Ks in autophagy or Mtb survival in macrophages has not been extensively studied. However, since PI4P is the first intermediate in the biosynthesis of PI(3,4,5)P3, a possible scenario is that that inhibition of PI4KB by clionamines or NPE71 would inhibit the formation of the autophagy blocker PI(3,4,5)P3, thereby releasing the autophagy brake and activating xenophagy to destroy Mtb in macrophages. Regardless of the exact link between inhibition of PI4KB and Mtb survival in macrophages, the current work has identified PI4KB as a new molecular target and CADs such as the clionamines, NPE71, and fluoxetine as a promising chemical group, that both merit further exploration as part of efforts to develop new HDT drugs for treatment of TB. This study illustrates the value of determining the molecular target of a natural product drug lead discovered using phenotypic assays as a path to revealing an unexploited cellular target for drug development.

SIGNIFICANCE

Infection with Mtb resulting in TB is the world's leading cause of death from an infectious bacterial disease. Standalone or adjuvant HDTs have advantages in killing Mtb strains that are drug resistant and is less likely to promote development of new resistant strains. This work showed that the natural product clionamines inhibit the survival of Mtb in macrophages in a host-directed manner. Yeast chemical-genetic profiling, a biotinylated clionamine probe pulldown experiment, and a yeast cell-based assay for inhibition of PI4P production in the TGN all support the Pik1 PI4 kinase as a cellular target of the clionamines. The chemical-genetic profiles and structures of clionamines are typical of CADs and this work has linked the Mtb inhibition phenotype elicited by clionamines to their CAD properties and co-localization with PI4P in a vesicular compartment. siRNA knockdown of PI4KB, the mammalian homolog of yeast *PIK1*, inhibited the survival of Mtb in macrophages, identifying PI4KB as an unexplored molecular target for HDT treatment of TB.

STAR★METHODS

Detailed methods are provided in the online version of this paper and include the following:

- KEY RESOURCES TABLE
- RESOURCE AVAILABILITY
  - Lead contact
  - Materials availability
  - Data and code availability

SUPPLEMENTAL INFORMATION

Supplemental information can be found online at https://doi.org/10.1016/j.chembiol.2021.07.017.

ACKNOWLEDGMENTS

Financial support was provided by the Canadian Institutes of Health Research PJT-148646 (Y.A.) and PJT-152931 (Y.A. and R.A.) and FDN-143264 (C.B.), the TB Veterans Association (Y.A.), NSERC (R.A.), the Ontario Ministry of Research and Innovation RE09-011 (C.B.), and the Canada Foundation for Innovation Project #36441 (C.B.). C.B. and Y.Y. were supported by MEXT KAKENHI grant number JP17H06411. S.C.L. was supported by a RIKEN Foreign Postdoctoral Research Fellowship and a RIKEN Incentive Research Projects Grant. We acknowledge the Chemical Resource Development Research Unit, Technology Platform Division, RIKEN CSRS for providing the NPDepo compound. Zhijian Li, Guihong Tan, and Bryan San Luis constructed the yeast drug-hypersensitive TS mutant and MoBY overexpression libraries. Jacqueline Barber generated the diagnostic mutant profile for RP-3-161. Sequencing was provided by Genome Network Analysis Support Facility (GeNAS), RIKEN Center for Life Science Technologies. Scott Simpkins and Justin Nelson provided computational analysis for quantifying the CG interactions. Carla Zimmerman and Urvi Bhojoo provided technical assistance.

AUTHOR CONTRIBUTIONS

Conceptualization, R.J.A., M.R., C.B., Y.A.-G., C.J.R.L., A.-C.G., S.C.L., R.P., and J.D.C.; methodology, M.R., C.B., S.C.L., C.J.R.L., X.Z., Y.A.-G., J.D.C., R.F., A.C.G., and R.P.; investigation, R.P., S.C.L., J.D.C., R.F., Y.Y., M.Y., J.T.C., X.Z., A.D.B., and E.D.; writing – original draft, R.J.A., M.R., Y.A.-G., S.C.L., J.D.C., C.B., A.C.G., and C.J.R.L.; writing – review & editing, R.J.A., M.R., Y.A.-G., C.B., S.C.L., Y.Y., J.D.C., C.J.R.L., and R.P.; funding acquisition, R.J.A., M.R., Y.A.-G., C.B., Y.Y., C.J.R.L., and A.-C.G.; resources, R.J.A., M.R., Y.A.-G., C.B., C.J.R.L., and A.-C.G.; supervision, R.J.A., M.R., Y.A.-G., C.B., C.J.R.L., and A.C.G.

DECLARATION OF INTERESTS

The authors declare no competing interests.

Received: April 2, 2021
Revised: June 16, 2021
Accepted: July 21, 2021
Published: September 13, 2021

REFERENCES

Bach, H., Papavinasasundaram, K.G., Wong, D., Hmama, Z., and Av-Gay, Y. (2008). *Mycobacterium tuberculosis* virulence is mediated by PtpA dephosphorylation of human VPS33B. Cell Host Microbe *3*, 316–322.

Balgi, A.D., Fonseca, B.D., Donohue, E., Tsang, T.C.F., Lajoie, P., Proud, C.G., Nabi, I.R., and Roberge, M. (2009). Screen for chemical modulators of autophagy reveals novel therapeutic inhibitors of mTORC1 signaling. PLoS One *49*, e7124.

Baradaran-Heravi, A., Balgi, A.D., Zimmerman, C., Choi, K., Shidmoossavee, F.S., Tan, J.S., Bergeaud, C., Krause, A., Flibotte, S., Shimizu, Y., et al. (2016). Novel small molecules potentiate premature termination codon readthrough by aminoglycosides. Nucleic Acids Res. *44*, 6583–6598.

Bennett, M., Onnebo, S.M.N., Azevedo, C., and Saiardi, A. (2006). Inositol pyrophosphates: metabolism and signaling. Cell. Mol. Life Sci. *63*, 552–564.

Burda, P., Padilla, S.M., Sarkar, S., and Emr, S.D. (2002). Retromer function in endosome-to-Golgi retrograde transport is regulated by the yeast Vps34 PtdIns 3-kinase. J. Cell Sci. *115*, 3889–3900.

Chee, C.B.E., Reves, R., Zhang, Y., and Belknap, R. (2018). Latent tuberculosis infection: opportunities and challenges. Respirology *23*, 893–900.

Choi, S.W., Gu, Y., Peters, R.S., Salgame, P., Ellner, J.J., Timmins, G.S., and Deretic, V. (2018). Ambroxol induces autophagy and potentiates rifampin antimycobacterial activity. Antimicrob. Agents Chemother. *62*, e01019–18.

Costanzo, M., Baryshnikova, A., Bellay, J., Kim, Y., Spear, E.D., Sevier, C.S., Ding, H., Koh, J.L.Y., Toufighi, K., Mostafavi, S., et al. (2010). The genetic landscape of a cell. Science *327*, 425–431.

Czajkowska, D., Morzycki, J.W., Santillan, R., and Siergiejczyk, L. (2009). Synthesis of "glycospirostanes" via ring-closing metathesis. Steroids *74*, 1073–1079.

Dalton, L.E., Bean, B.D.M., Davey, M., and Conibear, E. (2017). Quantitative high-content imaging identifies novel regulators of Neo1 trafficking at endosomes. Mol. Biol. Cell *28*, 1539–1550.

Deretic, V., Singh, S., Master, S., Harris, J., Roberts, E., Kyei, G., Davis, A., de Haro, S., Naylor, J., Lee, H.-L., and Vergne, I. (2006). *Mycobacterium tuberculosis* inhibition of phagolysosome biogenesis and autophagy as a host defence mechanism. Cell. Microbiol. *8*, 719–727.

Deutsch, E.W., Mendoza, L., Shteynberg, D., Farrah, T., Lam, H., Tasman, N., Sun, Z., Nilsson, E., Pratt, B., Prazen, B., et al. (2010). A guided tour of the Trans-Proteomic Pipeline. Proteomics *10*, 1150–1159.

Dheda, K., Gumbo, T., Maartens, G., Dooley, K.E., McNerney, R., Murray, M., Furin, J., Nardell, E.A., London, L., Lessem, E., et al. (2017). The epidemiology, pathogenesis, transmission, diagnosis, and management of multidrug-resistant, extensively drug-resistant, and incurable tuberculosis. Lancet Respir. Med. *5*, 291–360.

Du, L.L., and Novick, P. (2001). Yeast rab GTPase-activating protein Gyp1p localizes to the Golgi apparatus and is a negative regulator of Ypt1p. Mol. Biol. Cell *12*, 1215–1226.

Duan, L., Yi, M., Chen, J., Li, S., and Chen, W. (2016). *Mycobacterium tuberculosis* EIS gene inhibits macrophage autophagy through up-regulation of IL-10 by increasing the acetylation of histone H3. Biochem. Biophys. Res. Commun. *473*, 1229–1234.

Flanagan, C., Schnieders, E., Emerick, A., Kunisawa, R., Admon, A., and Thorner, J. (1993). Phosphatidylinositol 4-kinase: gene structure and requirement for yeast cell viability. Science *262*, 1444–1448.

Floto, R.A., Sarkar, S., Perlstein, E.O., Kampmann, B., Schreiber, S.L., and Rubinsztein, D.C. (2007). Small molecule enhancers of rapamycin-Induced TOR inhibition promote autophagy, reduce toxicity in Huntington's disease models and enhance killing of mycobacteria by macrophages. Autophagy *3*, 620–622.

Forestieiri, R., Donohue, E., Balgi, A., Roberge, M., and Andersen, R.J. (2013). Synthesis of clionamine B, an autophagy stimulating aminosteroid isolated from the sponge *Cliona celata*. Org. Lett. *15*, 3918–3921.

Fratti, R.A., Backer, J.M., Corvera, S., and Deretic, V. (2001). Role of phosphatidylinositol 3-kinase and Rab5 effectors in phagosomal biogenesis and mycobacterial phagosome maturation arrest. J. Cell Biol. *154*, 631–644.

Fratti, R.A., Chua, J., Vergne, I., and Deretic, V. (2003). *Mycobacterium tuberculosis* glycosylated phosphatidylinositol causes phagosome maturation arrest. Proc. Natl. Acad. Sci. U S A *100*, 5437–5442.

Giaever, G., Shoemaker, D.D., Jones, T.W., Liang, H., Winzeler, E.A., Astromoff, A., and Davis, R.W. (1999). Genomic profiling of drug sensitivities via induced haploinsufficiency. Nat. Genet. *21*, 278–283.

Gupta, A., Misra, A., and Deretic, V. (2016). Targeted pulmonary delivery of inducers of host macrophage autophagy as a potential host-directed chemotherapy of tuberculosis. Adv. Drug Deliver. Rev. *102*, 10–20.

Hendricks, K., Wang, B., Schnieders, E., and Thorner, J. (1999). Yeast homologue of neuronal frequenin is a regulator of phosphatidylinositol-4-OH kinase. Nat. Cell Biol. *1*, 234–241.

Ho, C.H., Magtanong, L., Barker, S.L., Gresham, D., Nishimura, S., Natarajan, P., Koh, J.L.Y., Porter, J., Gray, C.A., Andersen, R.J., et al. (2009). A molecular barcoded yeast ORF library enables mode-of-action analysis of bioactive compounds. Nat. Biotechnol. *27*, 369–377.

Hu, Y., Wen, Z., Liu, S., Cai, Y., Guo, J., Xu, Y., Lin, D., Zhu, J., Li, D., and Chen, X. (2020). Ibrutinib suppresses intracellular *Mycobacterium tuberculosis* growth by inducing macrophage autophagy. J. Infect. *80*, e19–e26.

Hua, Z., and Graham, T.R. (2003). Requirement for neo1p in retrograde transport from the Golgi complex to the endoplasmic reticulum. Mol. Biol. Cell *14*, 4971–4983.

Huttner, I., Strahl, T., Osawa, M., King, D., Ames, J., and Thorner, J. (2003). Molecular interactions of yeast frequenin (Frq1) with the phosphatidylinositol 4-kinase isoform, Pik1. J. Biol. Chem. *278*, 4862–4874.

Jiang, B., Shi, H., Tian, W., and Zhou, W. (2008). The convergent synthesis of novel cytotoxic certonardosterol D2 from disogenin. Tetrahedron *64*, 469–476.

Juarez, E., Carranza, C., Sanchez, G., Gonzalez, M., Chavez, J., Sarabia, C., Torres, M., and Sada, E. (2016). Loperamide restricts intracellular growth of *Mycobacterium tuberculosis* in lung macrophages. Am. J. Respir. Cell Mol. Biol. *55*, 837–847.

Kang, P.B., Azad, A.K., Torelles, J.B., Kaufman, T.M., Beharka, A., Tibesar, E., DesJardin, L.E., and Schlesinger, L.S. (2005). The human macrophage mannose receptor directs *Mycobacterium tuberculosis* lipoarabinomannan-mediated phagosome biogenesis. J. Exp. Med. *202*, 987–999.

Kaufmann, S.H.E., Dorhoi, A., Hotchkiss, R.S., and Bartenschlager, R. (2018). Host-directed therapies for bacterial and viral infections. Nat. Rev. Drug Discov. *17*, 35–56.

Keyzers, R.A., Daoust, J., Davies-Coleman, M.T., Van Soest, R., Balgi, A., Donohue, E., Roberge, M., and Andersen, R.J. (2008). Autophagy-modulating amino steroids isolated from the sponge *Cliona celata*. Org. Lett. *10*, 2959–2962.

Kihara, A., Noda, T., Ishihara, N., and Ohsumi, Y. (2001). Two distinct Vps34 phosphatidylinositol 3-kinase complexes function in autophagy and carboxypeptidase Y sorting in *Saccharomyces cerevisiae*. J. Cell Biol. *152*, 519–530.

Kim, J.-J., Lee, H.-M., Shin, D.-M., Kim, W., Yuk, J.-M., Jin, H.S., Lee, S.-H., Cha, G.-H., Kim, J.-M., Lee, Z.-W., et al. (2012). Host cell autophagy activated by antibiotics is required for their effective antimycobacterial drug action. Cell Host Microbe *11*, 457–468.

Kim, Y.S., Silwal, P., Kim, S.Y., Yoshimori, T., and Jo, E.-K. (2019). Autophagy-activating strategies to promote innate defense against mycobacteria. Exp. Mol. Med. *51*, 151.

Kimmey, J.M., and Stallings, C.L. (2016). Bacterial pathogens versus autophagy: implications for therapeutic interventions. Trends Mol. Med. *22*, 1060–1076.

Lam, K.K.Y., Zheng, X., Forestieri, R., Balgi, A.D., Nodwell, M., Vollett, S., Anderson, H.J., Andersen, R.J., Av-Gay, Y., and Roberge, M. (2012). Nitazoxanide stimulates autophagy and Inhibits mTORC1 signaling and intracellular proliferation of *Mycobacterium tuberculosis*. PLoS Pathog. *8*, e1002691. https://doi.org/10.1371/journal.ppat.1002691.

Lamb, C.A., Yoshimori, T., and Tooze, S.A. (2013). The autophagosome: origins unknown, biogenesis complex. Nat. Rev. Mol. Cell Biol. *14*, 759–774.

Lee, A.Y., St Onge, R.P., Proctor, M.J., Wallace, I.M., Nile, A.H., Spagnuolo, P.A., Jitkova, Y., Gronda, M., Wu, Y., Kim, M.K., et al. (2014). Mapping the cellular response to small molecules using chemogenomic fitness signatures. Science *344*, 208–211.

Lee, H.-J., Ko, H.-J., Kim, S.H., and Jung, Y.-J. (2019). Pasakbumin A controls the growth of *Mycobacterium tuberculosis* by enhancing the autophagy and production of antibacterial mediators in mouse macrophages. PLoS One *14*, e0199799.

Levine, B., Mizushima, N., and Virgin, H.W. (2011). Autophagy in immunity and inflammation. Nature *469*, 323–335.

Li, R. (1997). Bee1, a yeast protein with homology to Wiscott-Aldrich syndrome protein, is critical for the assembly of cortical actin cytoskeleton. J. Cell Biol. *136*, 649–658.

Li, Z., Vizeacoumar, F.J., Bahr, S., Li, J., Warringer, J., Vizeacoumar, F.S., Min, R., VanderSluis, B., Bellay, J., DeVit, M., et al. (2011). Systematic exploration of essential yeast gene function with temperature-sensitive mutants. Nat. Biotechnol. *29*, 361.

Liu, G., Zhang, J., Larsen, B., Stark, C., Breitkreutz, A., Lin, Z.-Y., Breitkreutz, B.-J., Ding, Y., Colwill, K., Pasculescu, A., et al. (2010). ProHits: integrated software for mass spectrometry-based interaction proteomics. Nat. Biotechnol. *28*, 1015–1017.

Machelart, A., Song, O.-R., Hoffmann, E., and Brodin, P. (2017). Host-directed therapies offer novel opportunities for the fight against tuberculosis. Drug Discov. Today *22*, 1250–1257.

Madania, A., Dumoulin, P., Grava, S., Kitamoto, H., Schärer-Brodbeck, C., Soulard, A., Moreau, V., and Winsor, B. (1999). The *Saccharomyces cerevisiae* homologue of human Wiskott-Aldrich syndrome protein Las17p interacts with the Arp2/3 complex. Mol. Biol. Cell *10*, 3521–3538.

Mitter, A.L., Schlotterhose, P., and Krick, R. (2019). Gyp1 has a dual function as Ypt1 GAP and interaction partner of Atg8 in selective autophagy. Autophagy *15*, 1031–1050.

Mizushima, N., Yoshimori, T., and Ohsumi, Y. (2011). The role of Atg proteins in autophagosome formation. Annu. Rev. Cell. Dev. Biol. *27*, 107–132.

NIH (2016). A 14 day early bactericidal activity study of nitazoxanide for the treatment of tuberculosis. ClinicalTrials.Gov.

O'Farrell, F., Rusten, T.E., and Stenmark, H. (2013). Phosphoinositide 3-kinases as accelerators and brakes of autophagy. FEBS J *280*, 6322–6337.

Paik, S., Kim, J.K., Chung, C., and Jo, E.-K. (2019). Autophagy: a new strategy for host-directed therapy of tuberculosis. Virulence *10*, 448–459.

Parsons, A.B., Brost, R.L., Ding, H., Li, Z., Zhang, C., Sheikh, B., Brown, G.W., Kane, P.M., Hughes, T.R., and Boone, C. (2004). Integration of chemical-genetic and genetic interaction data links bioactive compounds to cellular target pathways. Nat. Biotech. *22*, 62–69.

Piotrowski, J.S., Li, S.C., Deshpande, R., Simpkins, S.W., Nelson, J., Yashiroda, Y., Barber, J.M., Safizadeh, H., Wilson, E., Okada, H., et al. (2017). Functional annotation of chemical libraries across diverse biological processes. Nat. Chem. Biol. *13*, 982–993.

Ramon-Garcia, S., Ng, C., Anderson, H., Chao, J.D., Zheng, X., Pfeifer, T., Av-Gay, Y., Roberge, M., and Thompson, C.J. (2011). Synergistic drug combinations for tuberculosis therapy identified by a novel high-throughput screen. Antimicrob. Agents Chemother. *55*, 3861–3869.

Robinson, J.S., Klionsky, D.J., Banta, L.M., and Emr, S.D. (1988). Protein sorting in *Saccharomyces cerevisiae*: isolation of mutants defective in the delivery and processing of multiple vacuolar hydrolases. Mol. Cell. Biol. *8*, 4936–4948.

Saleh, M.T., and Belisle, J.T. (2000). Secretion of an acid phosphatase (SapM) by *Mycobacterium tuberculosis* that is similar to eukaryotic acid phosphatases. J. Bacteriol. *182*, 6850–6853.

Schindelin, J., Arganda-Carreras, I., Frise, E., Kaynig, V., Longair, M., Pietzsch, T., Preibisch, S., Rueden, C., Saalfeld, S., Schmid, B., et al. (2012). Fiji: an open-source platform for biological-image analysis. Nat. Methods *9*, 676–682.

Seaman, M., McCaffery, J., and Emr, S. (1998). A membrane coat complex essential for endosome-to-Golgi retrograde transport in yeast. J. Cell Biol. *142*, 665–681.

Seaman, M.N., Marcusson, E.G., Cereghino, J.L., and Emr, S.D. (1997). Endosome to Golgi retrieval of the vacuolar protein sorting receptor, Vps10p, requires the function of the VPS29, VPS30, and VPS35 gene products. J. Cell Biol. *137*, 79–92.

Shapira, T., Rankine-Wilson, L., Chao, J.D., Pichler, V., Rens, C., Pfeifer, T., and Av-Gay, Y. (2020). High-content screening of eukaryotic kinase inhibitors identify CHK2 inhibitor activity against *Mycobacterium tuberculosis*. Front. Microbiol. *11*, 553962.

Sharma, V., Verma, S., Seranova, E., Sarkar, S., and Kumar, D. (2018). Selective autophagy and xenophagy in infection and disease. Front. Cell Dev. Biol. *6*, article 147.

Shin, J.J.H., Liu, P., Chan, L.J., Ullah, A., Pan, J., Borchers, C.H., Burke, J.E., Stefan, C., Smits, G.J., and Loewen, C.J.R. (2020). pH Biosensing by PI4P regulates cargo sorting at the TGN. Dev. Cell *52*, 461–476.e4.

Shteynberg, D., Deutsch, E.W., Lam, H., Eng, J.K., Sun, Z., Tasman, N., Mendoza, L., Moritz, R.L., Aebersold, R., and Nesvizhskii, A.I. (2011). iProphet: multi-level integrative analysis of shotgun proteomic data improves peptide and protein identification rates and error estimates. Mol. Cell. Proteomics *10*, M111.007690.

Simpkins, S.W., Nelson, J., Deshpande, R., Li, S., Piotrowski, J.S., Wilson, E.H., Gebre, A.A., Safizadeh, H., Okamoto, R., Yoshimura, M., et al. (2018). Predicting bioprocess targets of chemical compounds through integration of chemical-genetic and genetic interactions. PLoS Comput. Biol. *14*, e1006532.

Simpkins, S.W., Deshpande, R., Nelson, J., Li, S.C., Piotrowski, J.S., Ward, H.N., Yashiroda, Y., Osada, H., Yoshida, M., Boone, C., et al. (2019). Using BEAN-counter to quantify genetic interactions from multiplexed barcode sequencing experiments. Nat. Protoc. *14*, 415–440.

Stanley, S.A., Barczak, A.K., Silvis, M.R., Luo, S.S., Sogi, K., Vokes, M., Bray, M.-A., Carpenter, A.E., Moore, C.B., Siddiqi, N., et al. (2014). Identification of host-targeted small molecules that restrict intracellular *Mycobacterium tuberculosis* growth. PLoS Pathog. *10*, e1003946.

Sun, J., Lau, A., Wang, X., Liao, T.-U.A., Zoubeidi, A., and Hmama, Z. (2009). A broad range of recombination cloning vectors in mycobacteria. Plasmid *62*, 158–165.

Takar, M., Wu, Y., and Graham, T.R. (2016). The essential Neo1 protein from budding yeast plays a role in establishing aminophospholipid asymmetry of the plasma membrane. J. Biol. Chem. *291*, 15727–15739.

Takar, M., Huang, Y., and Graham, T.R. (2019). The PQ-loop protein Any1 segregates Drs2 and Neo1 functions required for viability and plasma membrane phospholipid asymmetry. J. Lipid Res. *60*, 1032–1042.

Teo, G., Liu, G., Zhang, J., Nesvizhskii, A.I., Gingras, A.-C., and Choi, H. (2014). SAINTexpress: improvements and additional features in significance analysis of INTeractome software. J. Proteomics *100*, 37–43.

Tukey, J. (1977). Exploratory Data Analysis (Addison-Wesley Publishing Company).

Urbanek, A.N., Smith, A.P., Allwood, E.G., Booth, W.I., and Ayscough, K.R. (2013). A novel actin-binding motif in Las17/WASP nucleates actin filaments independently of Arp2/3. Curr. Biol. *23*, 196–203.

Vergne, I., Chua, J., and Deretic, V. (2003). Tuberculosis toxin blocking phagosome maturation inhibits a novel Ca^{2+}/calmodulin-PI3K hVPS34 cascade. J. Exp. Med. *198*, 653–659.

Vergne, I., Chua, J., Lee, H.H., Lucas, M., Belisle, J., and Deretic, V. (2005). Mechanism of phagolysosome biogenesis block by viable *Mycobacterium tuberculosis*. Proc. Natl. Acad. Sci. U S A *102*, 4033–4038.

Wallis, R.S., and Hafner, R. (2015). Advancing host-directed therapy for tuberculosis. Nat. Rev. Immun. *15*, 255–263.

Wang, S.-S., Shi, Y., and Tian, W.-S. (2014). Highly efficient and scalable synthesis of clionamine D. (2014). Org. Lett. *16*, 2177–2179.

Wong, D., Bach, H., Sun, J., Hmama, Z., and Av-Gay, Y. (2011). *Mycobacterium tuberculosis* protein tyrosine phosphatase (PtpA) excludes host vacuolar-H^+-ATPase to inhibit phagosome acidification. Proc. Natl. Acad. Sci. U S A *108*, 19371–19376.

Wicky, S., Schwarz, H., and Singer-Krüger, B. (2004). Molecular interactions of yeast Neo1p, an essential member of the Drs2 family of aminophospholipid translocases, and its role in membrane trafficking within the endomembrane system. Mol. Cell. Biol. *24*, 7402–7418.

Williams, D.E., and Andersen, R.J. (2020). Biologically active marine natural products and their molecular targets discovered using a chemical genetics approach. Nat. Prod. Rep. *37*, 517–633.

Winzeler, E.A., Shoemaker, D.D., Astromoff, A., Liang, H., Anderson, K., Andre, B., Bangham, R., Benito, R., Boeke, J.D., Bussey, H., et al. (1999). Functional characterization of the *S. cerevisiae* genome by gene deletion and parallel analysis. Science *285*, 901–906.

World Health Organization (2020). Tuberculosis. https://www.who.int/news-room/fact-sheets/detail/tuberculosis.

Young, C., Walzl, G., and Du Plessis, N. (2020). Therapeutic host-directed strategies to improve outcome in tuberculosis. Mucosal Immunol. *13*, 190–204.

Zhang, Q., Sun, J., Wang, Y., He, W., Wang, L., Zheng, Y., Wu, J., Zhang, Y., and Jiang, X. (2017). Antimycobacterial and anti-inflammatory mechanisms of baicalin via induced autophagy in macrophages infected with *Mycobacterium tuberculosis*. Front. Microbiol. *8*, 2142.

Zumla, A., Rao, M., Wallis, R.S., Kazufmann, S.H.E., Rustomjee, R., Mwaba, P., Vilaplana, C., Yeboah-Manu, D., Chakaya, J., Ippolito, G., et al. (2016). For the Host-Directed Therapies Network consortium. Host-directed therapies for infectious diseases: current status, recent progress, and future prospects. Lancet Infect. Dis. *16*, e47–63.

STAR★METHODS

KEY RESOURCES TABLE

REAGENT or RESOURCE	SOURCE	IDENTIFIER
Antibodies		
GFP antibody	Roche	Cat# 1181446001; RRID: AB_390913
Bacterial and virus strains		
M. tuberculosis H37Rv	Av-Gay Lab stock, University of British Columbia	NA
M. tuberculosis H37Rv pJAK2.A expressing luciferase	Plasmid constructed by Sun et al., (2009) and transformed into *M. tuberculosis* (Ramon-Garcia et al., 2011)	NA
M. tuberculosis H37Rv pTEC27 expressing RFP	Shapira et al., (2020)	Addgene 30,182
Chemicals, peptides, and recombinant proteins		
Middlebrook 7H9	BD	Cat#CA90003-876
BSA	Sigma Aldrich	Cat#A7906
Dextrose anhydrous	Fisher BioReagent	Cat#BP350-1
Catalase	Sigma Aldrich	Cat#c9322
Oleic acid	Sigma Aldrich	Cat#O1008
RPMI1640	Sigma Aldrich	Cat#R5886
Fetal Bovine Serum, qualified, heat inactivated	ThermoFisher	Cat#12484028
PBS	Gibco	Cat#14190144
Phorbol12-myristate13-acetate	Sigma Aldrich	Cat#P1585
Paraformaldehyde	ThermoFisher	Cat#28908
Hoechst 33,342, Trihydrochloride, Trihydrate	ThermoFisher	Cat#H1399
Thiazolyl Blue Tetrazolium Bromide	Sigma Aldrich	Cat#M2128
Bright-Glo luciferase reagent	Promega	Cat#E2610
HiPerFect transfection reagent (Qiagen)	Qiagen	Cat#301705
FastStart Universal SYBR Green Master (Rox)	Roche	Cat#4913850001
Yeast extract	Wisent Bio Products	Cat#800-150-DG
Peptone	Wisent Bio Products	Cat#800-157-DG
Galactose	Bishop	Cat#GAL502.1
Agar	Wisent Bio Products	Cat#800-010-DG
Platinum Taq Polymerase	Invitrogen	Cat#LS12532016
NPE71 (MolPort-002-893-643)	Maybridge	Cat#BTB12240
Fluoxetine	TargetMol	Cat#T0450
Critical commercial assays		
Illustra RNAspin minikit	GE Healthcare	Cat#25-0500-71
OneScript® Plus cDNA Synthesis Kit	Abm	Cat#G236
QIAamp 96 DNA Kit	Qiagen	Cat#51331
Geneclean III kit	MP Biomedicals	Cat# 111001600
KAPA Library Quantification kit	Roche	Cat#07960140001

(*Continued on next page*)

Continued

REAGENT or RESOURCE	SOURCE	IDENTIFIER
Experimental models: cell lines		
Human THP-1 (male)	ATCC	ATCC® TIB-202™
MCF7 (female)	ATCC	ATCC® HTB-22™
Experimental models: organisms/strains		
S. cerevisiae BY4741 GFP-Osh2-PH	Shin et al., (2020)	416-GFP-Osh2-PH
S. cerevisiae Pik1-104 GFP-Osh2-PH	Shin et al., (2020)	416-GFP-Osh2-PH
S. cerevisiae drug hypersensitive diagnostic mutant deletion library	pubmed.ncbi.nlm.nih.gov/28759014/	Diagnostic set
S. cerevisiae drug hypersensitive heterozygous diploid (HET) collection	Boone laboratory, University of Toronto	HET collection
S. cerevisiae drug hypersensitive temperature-sensitive conditional mutant collection	Boone laboratory, University of Toronto	TS collection
S. cerevisiae molecular barcoded Yeast (MoBY) overexpression collection	Boone laboratory, University of Toronto	MoBY overexpression collection
Oligonucleotides		
siRNA targeting sequence: Scrambled (Negative Control DsiRNA)	IDT	51-01-14-04
siRNA targeting sequence: PI4KB	IDT	hs.Ri.PI4KB.13.3
GAPDH For primer:GCCTCAAGA TCATCAGCAATGC	Av-Gay laboratory, University of British Columbia	N/A
GAPDH Rev primer:GTGGTCATGAG TCCTTCCACGA	Av-Gay laboratory, University of British Columbia	N/A
PI4KB For primer:TCGGAAACACA TGGACAAGG	Av-Gay laboratory, University of British Columbia	N/A
PI4KB Rev primer:GGAAGCAAGG AAGCTGAGAA	Av-Gay laboratory, University of British Columbia	N/A
Diagnostic, HET, and MoBY forward primer:AATGATACGGCGACCACCGAC ACTCTTTCCCTACACGACGCTCTTCC GATCTNNNNNNNNNNTGTCCACGA GGTCTCT	pubmed.ncbi.nlm.nih.gov/28759014/	N/A
Diagnostic, HET, and MoBY reverse primer: CAAGCAGAAGACGCATACGAGCTCTT CCGATCTGCACGTCAAGACTGTCAAGG	pubmed.ncbi.nlm.nih.gov/28759014/	N/A
TS forward primer: AATGATACGGCGA CCACCGAGATCTACACTCTTTCCCTA CACGACGCTCTTCCGATCTNNNNN NNNNNGGACATTGCCTTCTAGTTG	Boone laboratory, University of Toronto	N/A
TS reverse primer: CAAGCAGAAGAC GGCATACGAGCTCTTCCGATCTCC TTACTCCACTCGTCAT	Boone laboratory, University of Toronto	N/A
Software and algorithms		
ImageJ v2.0.0	Fiji Schindelin et al., 2012	RRID: SCR_003070; imagej.net/Fiji
GraphPad Prism v5.0f	Prism	RRID: SCR_002798; www.graphpad.com/scientific-software/prism/
GraphPad Prism v9.1.2	Prism	RRID: SCR_002798; cdn.graphpad.com/downloads/prism/9/InstallPrism9.msi
BEAN-counter v1.1.5	Simpkins et al., 2019	www.github.com/csbio/BEAN-counter
CG-TARGET v0.2	Simpkins et al., 2018	www.github.com/csbio/CG-TARGET

(*Continued on next page*)

Continued

REAGENT or RESOURCE	SOURCE	IDENTIFIER
Microsoft Excel for Mac v16.49	Microsoft	RRID: SCR_016137; www.microsoft.com/en-ca/microsoft-365/excel
Microsoft Excel 2019 for Windows v1808	Microsoft	RRID: SCR_016137; www.microsoft.com/en-ca/microsoft-365/excel
SAINTexpress v3.6.1	Teo et al., 2014	RRID: SCR_018562; saint-apms.sourceforge.net
ProHits Laboratory Information Management System	Liu et al., 2010	www.prohitsMS.com

RESOURCE AVAILABILITY

Lead contact

Further information and requests for resources and reagents should be directed to and will be fulfilled by the lead contact, Raymond Andersen (raymond.andersen@ubc.ca).

Materials availability

There are no restrictions to the availability of materials.

Data and code availability

1. All data reported in this paper will be shared by the lead contact on request.
2. This paper does not report original code.
3. Any additional information required to reanalyze the data reported in this paper is available from the lead contact upon request.

EXPERIMENTAL MODEL AND SUBJECT DETAILS

Bacterial strains and culture conditions

M. tuberculosis H37Rv was obtained from laboratory stocks. Mtb expressing the luciferase gene from the kanamycin resistant pJAK2.A (Mtb Luc) or Mtb H37Rv transformed with the hygromycin resistant pTEC27 plasmid expressing tomatoRFP (Mtb RFP) were grown in Middlebrook 7H9 supplemented with 10 % OADC (5% bovine albumin fraction, 2% dextrose, 0.004% catalase, 0.05% oleic acid and 0.8% sodium chloride solution), 0.05% Tween-80 and 20 μg/mL kanamycin or 50 μg/mL hygromycin B, respectively.

Cell lines

MCF-7 cells (female) stably transfected with pEGFP-LC3 (Balgi et al., 2009) were maintained in RPMI-1640 medium supplemented with 400mg/mLG418 and 10% (v/v) fetal bovine serum, 2 g/L sodium bicarbonate and 1 mM HEPES. The cells were cultured at 37°C, 5% CO_2 in a humidified environment. THP-1 cells (ATCC TIB-202) were maintained in RPMI1640 incomplete media (10% FBS, 2% glutamine, 1% non-essential amino acids). All incubations of THP-1 cells were performed at 37°C, 5% CO_2 in a humidified environment. The cells were not authenticated in our hands.

METHOD DETAILS

Autophagy assays

For determination of EGFP-LC3 puncta, MCF-7 cells stably expressing EGFP-LC3 were seeded in PerkinElmer View 96-well plates at 20,000 cells per well. Eighteen hours after seeding, compounds were added from a 10 mg/mL solution in DMSO to triplicate wells and untreated wells were exposed to an equivalent volume of DMSO (0.1%). After 4 hr incubation at 37°C, the cells were fixed with 3% (v/v) paraformaldehyde containing the DNA dye Hoechst 33,342 (500 ng/mL) for 15 min at room temperature. The fixed cells were rinsed once with phosphate-buffered saline (PBS) containing 1 mM $MgCl_2$ and 0.1 mM $CaCl_2$ and stored in the same medium at 4°C overnight. The plates were then read in a Cellomics Arrayscan VTI automated fluorescence imager. Images of 12 fields per well, corresponding to approximately 3200 cells per well were acquired using a 20× objective in the Hoechst 33,342 and GFP (XF-100 filter) channels. The compartment analysis algorithm was used to identify the nuclei, apply a cytoplasmic mask and quantitate EGFP-LC3 puncta. Additional experimental details are described in Balgi et al. (2009). For determination of EGFP-LC3 processing, 200,000 MCF-7 cells stably expressing EGFP-LC3 were seeded in 12 well plates in a volume of 1 mL. The cells were exposed to compounds or DMSO for 4 hr as above. The cells were harvested, lysed and subjected to automated capillary electrophoresis

western analysis as described (Baradaran-Heravi et al., 2016), using a GFP antibody (Roche, cat #1181446001, 1:100 dilution). The data is plotted in the Figures S1 and S2.

Mtb infection of THP-1 cells

The assay uses an Mtb H37Rv strain expressing a luciferase reporter gene. Luminescence produced upon addition of luciferin is an indication of the total amount of luciferase expressed by the Mtb and can be used as an indication of the metabolic status of the Mtb inside the cell.

THP-1 cells were centrifuged and gently resuspended in fresh RPMI incomplete media containing 40 ng/mL phorbol12-myristate13-acetate (PMA) for differentiation. Cells were seeded into 96-well clear flat-bottom plates (VWR) at 100,000 cells/well in 200 μL of media and differentiation was allowed to proceed overnight. Mtb cultures grown to OD_{600} 0.3–0.5 were washed three times with 7H9-Tween-80 and resuspended in RPMI containing 10% human serum at a density of 2×10^8 cells/mL. Cells were incubated for 30 min at 37°C for opsonization to occur. THP-1 cells were washed twice with RPMI1640 then incubated with opsonized Mtb Luc (for dose response assays) or Mtb RFP (for siRNA assays) for 3 hr at a multiplicity of infection (MOI) of 5:1 or 2:1, respectively. Following infection, THP-1 cells were washed twice with RPMI1640. RPMI1640 incomplete media containing serial dilutions of compounds in DMSO or Rifampicin or DMSO controls were added to each well and cells were incubated for 3 days. For the luciferase assay, cells were washed with RPMI1640, followed by addition of 100 μL PBS and 50 μL luciferase reagent (Bright-Glo Luciferase Assay System) to each well. The plate was incubated for 5 min at room temperature according to the supplied protocol then scanned using a Biotek Synergy HT microplate reader. Data from dose-response assays were normalized using DMSO as a negative control, corresponding to 100% bacterial growth, and 20 μM rifampicin as a positive control, corresponding to 100% inhibition of bacterial growth. Error bars represent the SEM of two separate experiments done in triplicate and are representative of two additional experiments for RP-3-161. Non-linear regression was used to fit the data of the log (inhibitor) vs. response (variable slope) curve. For siRNA assays, cells were washed twice with RPMI1640, fixed with 4% paraformaldehyde (PFA) in warm PBS for 1 hr, then stained with 1 μg/mL Hoechst 33,342 in RPMI1640. The stain was removed after 15 min and cells were kept in PBS for scanning with a CellInsight CX5 HCS Platform (Thermo Scientific). The HCS Studio (Thermo Scientific) built-in software was used to calculate the average fluorescent area per infected THP-1 cell. Survival of Mtb in PI4KB siRNA-transfected THP-1 cells (see below) was calculated as a percentage of the fluorescence from the scrambled siRNA control after subtracting average fluorescence of the Rifampicin positive control corresponding to 100% killing (background). Statistics were performed using a two-tailed t test compared to the scrambled siRNA control. Error bars represent the SEM of experiments done in quadruplicate and are representative of three separate experiments. All data were normalized using Microsoft Excel and analyzed using GraphPad Prism software.

siRNA knockdown

THP-1 cells, seeded at 50,000 cells/well in 96-well plates, were differentiated overnight as above. Cells were gently washed twice with RPMI1640 to remove PMA followed by addition of 30 μL of RPMI incomplete media to each well. Transfection complex formation was performed following the traditional protocol as supplied by the manufacturer as follows: 0.1 μL (10 pmole) of siRNA (IDT) was added to 27.9 μL of RPMI1640, to which 2 μL of HiPerFect transfection reagent (Qiagen) was added, vortexed and incubated at room temperature for 9 min (volumes were scaled according to the number of replicates). The transfection complex (30 μL) was added to each well for a total of 60 μL per well. Cells were incubated for 5 hr at 37°C, 5% CO_2 in a humidified environment, after which 140 μL of RPMI incomplete media was added to each well to give a final siRNA concentration of 50 nmol/well. Cells were further incubated overnight before washing and infection with *M.tb* the following day as described above.

Quantitative real-time PCR

RNA from six to eight samples of THP-1 cells transfected with siRNA for 24 hr as above was extracted, combined and cleaned using the Illustra RNAspin Mini RNA Isolation Kit (GE Healthcare) according to the supplied protocol. Reverse transcription reactions were carried out in 20-μL volumes containing 250 ng RNA, oligo dT primers, and the buffer and enzyme components of the OneScript® Plus cDNA Synthesis Kit (ABM) according to the supplied protocol. Real-time PCR analysis was carried out on the CFX96 Real-Time System (BIO-RAD). Real-time qPCR reactions were carried out in 20-μL volumes containing 2X FastStart SYBR green master mix (Roche), 5 μL of 5-fold diluted cDNA and 0.3 μM of each primer. Control reactions without reverse transcriptase were included with each run to confirm the absence of genomic DNA contamination. Expression levels were normalized to the GAPDH gene. All primers were ordered from IDT.

Compound cytotoxicity assay

THP-1 survival exposed to increasing concentrations of compound was measured using an MTT assay. THP-1 cells were differentiated as above, washed and serial dilutions of compounds in DMSO were added. Cells were incubated in the presence of compounds or Rifampicin or DMSO controls for 3 days. Wells were replaced with 100 μL RPMI incomplete including 12.5 μL of 10 mg/mL MTT (Thiazolyl Blue Tetrazolium Bromide) and cells were incubated a further 2.5 h. Cells were lysed by adding 100 μL of extraction buffer (20% w/v of SDS dissolve in 50% N, N-dimethylformamide containing 2.5% acetic acid and 2.5% 1 M HCl) and incubated overnight. Plates were read on a VarioSkan™ Plate Reader at 570 nm. Data were normalized to DMSO as a negative

control corresponding to 100% THP-1 survival. Non-linear regression was used to fit the data of the log (inhibitor) vs. response (variable slope) curve using GraphPad Prism analysis software. Error bars represent the SEM of two separate experiments done in triplicate.

Drug hypersensitive, DNA barcoded *S. cerevisiae* mutant libraries

Detailed lists and genotypes for each mutant collection are in the supplemental information.

Diagnostic set

A set of 310 non-essential gene deletion mutants were selected for the diagnostic collection, as previously described (Piotrowski et al., 2017). The collection was constructed in a drug hypersensitive *MAT***a** *pdr1Δpdr3Δsnq2Δ* genetic background using SGA technology. The *MATα pdr1Δ::natMX pdr3Δ::KI.URA3 snq2Δ::KI.LEU2 can1Δ::STEpr-Sp_his5 lyp1Δ* (Y13206) query strain carries SGA markers, *can1Δ::STEpr-Sp_his5 lyp1Δ*. Y13206 was crossed to an array of *MAT***a** *xxxΔ::kanMX* deletion mutants (EUROSCARF) and, following SGA analysis, *MAT***a** *pdr1Δ::natMX pdr3Δ::KI.URA3 snq2Δ::KI.LEU2 xxxΔ::kanMX his3Δ1 leu2Δ0 ura3Δ0 met15Δ0* deletion mutants were isolated. The diagnostic collection contained UP and DOWN barcodes flanking the *kanMX* deletion cassette (Winzeler et al., 1999).

Heterozygous diploid (HET) collection

A set of 968 barcoded diploid heterozygous mutants, each containing half the gene copy of a unique essential gene, was constructed in yeast strain Y14486 *MAT***a**/*MATα pdr1Δ::natMX/pdr1Δ::natMX pdr3Δ::KI.URA3/pdr3Δ::KI.URA3 snq2Δ::KI.LEU2/snq2Δ::KI.LEU2 his3Δ1/his3Δ1 leu2Δ0/leu2Δ0 ura3Δ0/ura3Δ0 met15Δ0/met15Δ0*. Oligonucleotide primers were designed to generate *kanMX*-marked deletions of essential genes, and incorporate 20 bp barcodes upstream of each marked deletion. Diploid transformants were selected on YPD (1% yeast extract, 2% peptone, 2% glucose) media containing G418 (200 μg/mL), and the presence of desired deletions was confirmed by PCR. If we delete a given gene XXX, the resultant heterozygous diploid genotype would be *MAT***a**/*MATα xxxΔ::kanMX/XXX snq2Δ::KI.LEU2/snq2Δ::KI.LEU2 pdr3Δ::KI.URA3/pdr3Δ::KI.URA pdr1Δ::hygB/pdr1Δ::hygB can1Δ::STE2pr-Sp_his5/can1Δ::STE2pr-Sp_his5 lyp1Δ/lyp1Δ his3Δ1/his3Δ1 leu2Δ0/leu2Δ0 ura3Δ0/ura3Δ0 met15Δ0/met15Δ0.*

Temperature sensitive (TS) conditional mutant collection: First, a drug-hypersensitive, barcoded set of temperature-sensitive mutants was constructed for 1181 TS alleles covering 837 essential genes. A drug-hypersensitive, SGA-compatible ''barcoder collection'' was constructed. The *KI.URA3* marker in Y14478 (*MATα snq2Δ::KI.LEU2 pdr3Δ::KI.URA3 pdr1Δ::hygB can1-Δ::STE2pr-Sp_his5 lyp1Δ his3Δ1 leu2Δ0 ura3Δ0 met15Δ0*) was replaced by a *natMX* cassette. To make the barcoded drug hypersensitive TS mutant library, the above barcoder collection was mated to a G418-resistant ordered array of conditional temperature sensitive (TS) allele mutants. Serial rounds of plating on selective media isolated *MAT***a** haploids with the *pdr3*, *pdr1*, and *snq2* deletion alleles as well as the *kanMX*-marked TS allele and *natMX*-marked barcode (*MAT***a** *ts allele::kanMX pdr3Δ::natMX::barcode snq2Δ::KI.LEU2 pdr1Δ::hygB can1Δ::STE2pr-Sp_his5 lyp1Δ his3Δ1 leu2Δ0 ura3Δ0 met15Δ0*).

Molecular barcoded Yeast (MoBY) overexpression collection: A collection of 960 strains transformed with barcoded 2 micron plasmids (p5587), each expressing a unique yeast open reading frame (Ho et al., 2009), was constructed using a drug hypersensitive parent strain Y14475. (*MAT***a** *snq2Δ::KI.LEU2 pdr3Δ::KI.URA3 pdr1Δ::natMX can1Δ::STE2pr-Sp_his5 lyp1Δ his3Δ1 leu2Δ0 ura3Δ0 met15Δ0*)

Chemical-genetic profiling

Pooled yeast mutant libraries were treated with RP-3-161 as previously described (Piotrowski et al., 2017). Diagnostic, temperature sensitive (TS), heterozygous diploid (HET) and overexpression (MoBY) libraries were each pooled and distributed into separate wells in 96-well plates. Each well contained 4.65×10^5/mL cells, 196 μL YPGal medium (1% yeast extract, 2% peptone, 2% galactose) and 2 μL compound (RP-3-161, NPE-71, clionamine B, or fluoxetine) at different concentrations (3 μg/mL to 5 mg/mL stock solutions dissolved in DMSO, corresponding to a final working concentration range of 0.03 μg/mL to 50 μg/mL). OD_{600} was measured after 24 h using a plate reader, at which point the percentage of growth inhibition relative to the DMSO-only control (1% DMSO) was calculated to measure cell growth. This was followed by incubation for an additional 24 h at 30°C. The plates were then centrifuged at 3,000 rpm for 4 min before adding 125 μL zymolyase dissolved in 1 M D-sorbitol (final concentration: 0.5 mg/mL) with 11.5 μM β-mercaptoethanol. The samples were incubated for 1 h at 37°C, centrifuged again at 4,000 rpm for 5 min and processed using the QIAamp 96 DNA kit. Genomic DNA extraction was performed with an automated high-throughput nucleic acid purification robot, QIAcube HT (QIAGEN).

Strain-specific DNA barcodes were amplified using multiplex primers and a communal U2 primer. PCR conditions were set as follows: 3 min at 95°C for initial denaturation, 30 cycles of 15 s at 95°C, 15 s at 60°C, 20 s at 72°C, and a final extension time of 5 min at 72°C. PCR products were purified from 2% agarose gels using a Geneclean III kit, quantified using a Kapa qPCR kit and sequenced with a Hiseq 2500 machine at the RIKEN Center for Life Science Technologies (Yokohama, Japan).

Data processing

Chemical-genetic interaction z-scores normalized against DMSO-only (1% DMSO) treated samples were generated from amplicon sequencing data using the BEAN-counter software pipeline [github.com/csbio/BEAN-counter (Simpkins et al., 2019)]. The complete scoring method can be found in the Supplementary Note of Piotrowski et al., 2017. The screens were performed in separate batches

for each mutant library: each batch was processed and analyzed independently using BEAN-counter software. Chemical-genetic (CG) interaction z-scores normalized against DMSO-only (1% DMSO) treated samples were calculated from amplicon sequencing data, representing the standard deviation of each strain in the compound-treated profile with respect to its counterpart strain in the reference DMSO profile. Scatter plots of chemical-genetic profiles were generated on Excel. High confidence biological process target predictions (FDR<25%) were made for diagnostic set profiles using CG-TARGET software [github.com/csbio/CG-TARGET (Simpkins et al., 2018)], using process predictions from DMSO-only and randomized profiles for normalization.

Liquid growth assay

Overnight yeast cultures grown in SC media were diluted to OD600 = 0.2 in a 96-well flat bottom plate. The plate was incubated in a microplate reader (Epoch 2 by Biotek) at 30°C with shaking, and an automated program recorded OD600 readings every 4 min. Doubling times were calculated from non-linear fit of the growth curves with $R^2 > 0.98$.

Log phase live yeast cells grown in SC media (6.7 g/L yeast nitrogen base without amino acids, 2% glucose, 2 g/L complete amino acid supplement) exposed to RP-3-161 and NPE-71 were imaged using the Olympus Fluoview FV1000 laser scanning confocal microscope with the UplanSApo 100X/1.40 Oil immersion lens. Optical slices were taken from the centre of the cell using identical microscopy settings. Images were processed using the Fiji package of ImageJ (NIH).

Compound pull-down

Yeast cells BY4741 and BY4741 overexpressing PIK1 from a 2 micron plasmid p5889 (Ho et al., 2009) were harvested from 1L culture in log phase (OD 600 <0.8). Pellets were resuspended 1:1 (g:mL) in yeast lysis buffer [50 mM Tris-HCl pH 7.5, 150 mM NaCl, 5 mM EDTA, supplemented by fresh addition of 0.1% NP-40, 1x Roche complete protease inhibitors cocktail (cat#11836170001) and 5 mM DTT]. Lysis was performed by vortexing with 0.5 mm glass beads, and the lysate was collected by centrifugation at 14,000 r.p.m. for 20 min (4 °C).

Streptavidin-sepharose beads (GE Healthcare 17-5113-01), 15 μl packed beads per sample, were washed three times in PBS and resuspended in 100 μl PBS. 100 nmol of biotinylated compound in DMSO (RP-3-161 or cholesterol) was then added per sample to the streptavidin bead suspension and allowed to pre-bind the beads for ~2 h on a nutator at 4°C. The beads were washed three times with lysis buffer to remove unbound biotinylated compound before being incubated with lysates. 2 mL of lysate (~15 mg of total protein) was added to the beads and incubated on a nutator for 3 hours. Beads were then pelleted by centrifugation at 1,000 r.p.m. for 1 min using a small table-top microfuge and placed on a cold magnetic rack (placed on ice) to collect the beads on the tubes' sides. The supernatant was removed slowly with a pipette and the beads were resuspended in 3 × 0.5 mL of cold lysis buffer. The beads were transferred to a fresh 1.7 mL tube and washed three more times with 0.5 mL of 50 mM ammonium bicarbonate pH 8. Following the last wash, the samples were quickly centrifuged and the last drops of liquid were removed with a fine pipette.

The dried beads were resuspended in 5 μL of 50 mM ammonium bicarbonate pH 8 containing 1 μg of trypsin (Sigma, T7575) and the mixture was incubated at 37 °C with agitation overnight (~15 h). The sample was then magnetized and the supernatant was transferred to a fresh tube. Another 500 ng of trypsin was added (in 5 μL of 50 mM ammonium bicarbonate pH 8), and the resulting sample was incubated at 37 °C for 3–4 h without agitation. Formic acid was added to the sample to a final concentration of 2% (from 50% stock solution), and the sampled was dried in a vacuum centrifuge and stored at −40 °C until ready for mass spectrometric analysis.

Mass spectrometry analysis

Samples resuspended in 18 μL 2% formic acid were analyzed on the AB SCIEX 5600 TripleTOF in Data Dependent Acquisition (DDA) mode. 5 μL of the digested sample was analyzed using a homemade emitter column (75 μm × 10 cm) using Dr. Maisch Reprosil C_{18} 3 μm material. The column was coupled to a NanoLC-Ultra 1D plus (Eksigent, Dublin, CA) system with 0.1% formic acid in water as buffer A and 0.1% formic acid in ACN as buffer B. Samples were loaded on the column for 10 min at 400 nL/min (2% buffer B). The flow rate was then decreased to 200 nL/min and the HPLC delivered an acetonitrile gradient over 120 min (2–35% buffer B over 90 min, 40–60% buffer B over 5 min, hold buffer B at 80% 5 min, return to 2% B over 5 min and re-equilibrate the column for 15 min at 2% B). The DDA parameters were 1 MS scan (250 ms; mass range 400–1250) followed by up to 50 MS/MS scans (50 ms each). Candidate ions between charge states 2–5 and above a minimum threshold of 200 counts per second were isolated using a window of 0.7 a.m.u. Previous candidate ions were dynamically excluded for 20 s with a 50 mDa window.

The raw mass spectrometry files were stored, searched and analyzed using the ProHits laboratory information management system (LIMS) (Liu et al., 2010). The WIFF data files were converted to MGF format using WIFF2MGF and subsequently converted to an mzML format using ProteoWizard (3.0.4468) and the AB SCIEX MS Data Converter (V1.3 beta). The mzML files were searched using Mascot (v2.3.02) and Comet (2014.02 rev.2). The results from each search engine were jointly analyzed through TPP (the Trans-Proteomic Pipeline (Deutsch et al., 2010), (v4.7) via the iProphet pipeline (Shteynberg et al., 2011). The searched database contained the *S. cerevisiae* complement of the RefSeq protein database (version 57; 12,044 forward and reverse (decoy) entries searched).

The database parameters were set to search for tryptic cleavages, allowing up to 2 missed cleavage sites per peptide, MS1 mass tolerance of 35 ppm with charges of 2 + to 4+ and an MS2 mass tolerance of +/− 0.15 amu. Asparagine/glutamine deamidation and methionine oxidation were selected as variable modifications.

To identify significant interaction partners from the affinity purification data, the data were subjected to Significance Analysis of INTeractome express (SAINTexpress 3.6.1) analysis (Teo et al., 2014) implemented in ProHits. A full set of interactors meeting the SAINTexpress 1% FDR threshold are in Table S2.

Chemistry experimental section

Experimental methods

General details. All reactions requiring anhydrous conditions were carried out under an atmosphere of argon in oven-dried glassware. Anhydrous tetrahydrofuran (THF), dichloromethane (DCM), 1,2-dichloroethane (DCE), 1,2-dimethoxyethane (DME), methanol (MeOH), and toluene were commercially obtained. All other solvents were used as obtained. All starting materials were obtained commercially and were used without further purification unless otherwise indicated.

Thin-Layer Chromatography was carried out on aluminum-backed plates pre-coated with silica (60 F254, Merck) and visualized by immersion in *p*-anisaldehyde solution followed by heating. Purification of reaction products was carried out by flash column chromatography using silica gel (SiliCycle F60, 40-63μm) in the solvent systems indicated.

^{1}H and ^{13}C NMR Spectra were recorded using a Brüker AV600 spectrometer equipped with a 5 mm TCI or QNP cryoprobe. Chemical shifts are reported in ppm and referenced to internal residual chloroform ($CHCl_3$) at 7.26 ppm for ^{1}H NMR spectra, and to the central line of the deuterated chloroform ($CDCl_3$) triplet at 77.0 for ^{13}C NMR spectra; the central line of the deuterated dichloromethane (CD_2Cl_2) triplet at 5.32 for ^{1}H NMR spectra, and to the central line of the CD_2Cl_2 quintet at 54.0 for ^{13}C NMR spectra; the central line of the deuterated dimethyl sulfoxide (DMSO-d_6) quintet at 2.50 for ^{1}H NMR spectra, and to the central line of the DMSO-d_6 septet at 39.5 for ^{13}C NMR spectra. Coupling constants, *J*, are given in Hz to the nearest 0.1 Hz. The multiplicity of each signal is reported as s, d, t, q, quin, m, br denoting singlet, doublet, triplet, quartet, quintet, multiplet and broad, respectively.

High-resolution and low-resolution mass spectra were obtained by electrospray ionisation (ESI) using Waters ZQ LC-MS, Brüker Esquire LC and Waters microTOF; values are quoted as ratios of mass:charge (*m/z*) in Daltons.

Abbreviations used: TBDPSCl, tert-butyldiphenylchlorosilane; DMAP, N,N-dimethylpyridin-4-amine; DIBAL, diisobutylaluminum hydride; pTSA, 4-methylbenzenesulfonic acid; PVP, poly(4-vinylpyridine); TPP, 5,10,15,20-tetraphenyl-21H,23H-porphine; TBAF, tetrabutylammonium fluoride; DMP, Dess-Martin periodinane.

Optimized synthesis of clionamine B (2)

The optimized synthesis of clionamine B (Scheme S1) started from the readily available sapogenin tigogenin (**SI1**) using the general procedures described below. Degradation of the tigogenin (**SI1**) side chain to the give the γ-lactone **SI2** was accomplished in high yield by reaction at rt using excess peroxyacetic acid in the presence of iodine and sulfuric acid (Jiang et al., 2008; Czajkowska et al., 2009). Mild hydrolysis of the acetate ester **SI2** with MeOH and K_2CO_3 at rt gave the secondary alcohol **SI3** that was protected as the TBDPS (*tert*-butyldiphenylsilyl) ether to give **SI4**. Reduction of the lactone **SI4** with DIBAL at −78°C gave the hemiacetal **SI5** that was dehydrated with para-toluene sulfonic acid in refluxing toluene to give the enol ether **SI6**. A Schenck ene reaction resulting from incandescent lightbulb irradiation of a CH_2Cl_2 solution of enol **SI6** and catalytic *meso*-tetraphenylporphine purged with O_2 gave an intermediate C-21 hydroperoxy hemiacetal that was converted without isolation into the γ-methylene lactone **SI7** via treatment with acetic anhydride and triethylamine. Copper (I) catalyzed conjugate addition of isopentyl magnesium bromide to the α-methylene lactone **SI7** installed the steroidal side chain found in clionamine B (**2**) to give **SI8**. The C-21 hydroxyl was added by bubbling oxygen through a solution of lactone **SI8**, triethyl phosphite, and *t*-BuOH in DMF at −10°C followed by workup with aqueous HCl. NOE experiments confirmed that the hydroxyl group at C-21 in **SI9** was added from the least sterically hindered α face. Treatment of **SI9** with TBAF in refluxing THF removed the TBDPS protecting group to give the secondary alcohol **SI10** that was oxidized to the ketone **SI11** using Dess Martin periodinane (DMP). Reductive amination of **SI11** with NH_4OAc and $NaBH_3CN$ in MeOH gave clionamine B (**2**) identical in all respects to the natural product in 11 steps and 2.9% overall yield. Ketone **SI11** was also converted into the C-3 benzylamine derivative RP-3-161 (**5**) by reductive amination with benzyl amine and $NaBH(OAc)_3$.

General procedures for synthesis of clionamine analogs

Procedure A: oxidative degradation of spiroketal

I_2 (30.5 mg, 0.12 mmol) was added to a mixture of H_2SO_4 (54.2 μL) and acetic acid (3.33 mL) and stirred for 30 min at room temperature. Steroidal sapogenin, either tigogenin or sarsasapogenin (416.6 mg, 1.0 mmol), was then added to the resulting solution. After stirring for 10 min at room temperature, peroxyacetic acid solution (40% in acetic acid, 1.10 mL, 6.0 mmol) was added dropwise and the reaction mixture stirred for 24 hr. The pH of the mixture was then adjusted to ≈ pH 5 using aqueous 10% HCl which was added slowly, dropwise. The mixture was extracted with EtOAc (3 × 30 mL), the combined organic extracts dried ($MgSO_4$), filtered, and concentrated under reduced pressure. The residue was then purified by Si Gel flash column chromatography.

Procedure B: saponification of acetate

K_2CO_3 (276.4 mg, 2 mmol) was added to a solution of sapogenin acetate (388.6 mg, 1 mmol) in methanol (30 mL). The reaction mixture was stirred for 36 hr at room temperature, after which time it was concentrated to a few mL, redissolved in CH_2Cl_2 (20 mL) and H_2O (15 mL) was added. The mixture was then extracted with CH_2Cl_2 (3 × 10 mL), the combined organic extracts were dried ($MgSO_4$), filtered and concentrated under reduced pressure. The residue was then purified by Si Gel flash column chromatography.

Procedure C: TBDPS protection

Imidazole (184.5 mg, 2.7 mmol), and *N*,*N*-dimethylpyridin-4-amine (6.2 mg, 0.051 mmol) were added to a solution of alcohol (1.0 mmol) in anhydrous CH_2Cl_2 (7 mL). After stirring for 10 min at room temperature, *tert*-butyldiphenylchlorosilane (435.8 mL, 412.3 mg, 1.5 mmol) was added dropwise. The mixture was then stirred for 4 hr at this temperature. MeOH (3 mL) was added and the mixture stirred for a further 2 hr. The reaction mixture was concentrated. The residue was re-dissolved in CH_2Cl_2 (25 mL)

and water (12 mL) was added. The mixture was extracted with CH_2Cl_2 (3 × 30 mL), the combined organic extracts dried (MgSO4), filtered and concentrated under reduced pressure. The residue was then purified by Si Gel flash column chromatography.

Procedure D: reduction of lactone carbonyl

Diisobutylaluminum hydride (1.0 M in cyclohexane, 1.20 mL, 1.2 mmol) was added dropwise over 10 min to a cooled solution of lactone (1.0 mmol) in anhydrous CH_2Cl_2 (3 mL) at −78°C. After stirring for 30 min at this temperature, a second portion of diisobutylaluminum hydride (1.0 M in cyclohexane, 0.50 mL, 0.5 mmol) was added dropwise over 10 min and the reaction mixture stirred for a further 30 min at −78°C. The reaction mixture was quenched with 0.25 mL EtOH, warmed to room temperature, then 10 mL saturated aqueous potassium sodium tartrate solution was added and the resulting mixture stirred for 4 hr at room temperature. The mixture was extracted with CH_2Cl_2 (4 × 15 mL), the combined organic extracts were dried ($MgSO_4$), filtered and concentrated under reduced pressure. The residue was then purified by Si Gel flash column chromatography.

Procedure E: dehydration

4-Methylbenzenesulfonic acid (16.0 mg, 0.084 mmol), poly(4-vinylpyridine) (12.6 mg, 0.12 mmol) and activated 3Å molecular sieves (8 beads) were added to a solution of tetrahydrofuranol (1.0 mmol) in anhydrous toluene (12 mL). The reaction mixture was stirred under reflux for 1.5 hr then cooled to room temperature. The mixture was then filtered through a plug of Celite, and filtrate concentrated under reduced pressure. The residue was then purified by Si Gel flash column chromatography.

Procedure F: formation of exo-methylene lactone

5,10,15,20-Tetraphenyl-21*H*,23*H*-porphine (2.9 mg, 4.8 μmol) and $NaHCO_3$ (58.7 mg, 0.69 mmol) were added to a solution of dihydrofuran (1.0 mmol) in cyclohexane (11 mL). The reaction mixture was stirred at room temperature under constant illumination from an incandescent lightbulb, with O_2 constantly being bubbled through the solution for 16 hr. The reaction mixture was then concentrated to dryness. The residue was dissolved in CH_2Cl_2 (3 mL) and acetic anhydride (0.22 mL, 199.1 mg, 1.95 mmol) and triethylamine (0.18 mL, 246.9 mg, 2.44 mmol) were added. This mixture was then stirred for 1 hr at room temperature followed by removal of the solvent under reduced pressure. The residue was then purified by Si Gel flash column chromatography.

Procedure G: conjugate addition of organocuprate

To Mg turnings (600 mg, 25 mmol), previously cleared of its oxide layer using sand-paper and oven dried, in anhydrous THF (25 mL) was added a crystal of I_2. A solution of alkyl bromide (2.00 mL, 20 mmol) in anhydrous THF (29 mL) was added, and the mixture stirred at room temperature until the purple color of iodine was no longer visible. The mixture was heated to reflux for 1 hr then cooled to room temperature. Anhydrous THF (9 mL) was added to a round-bottomed flask containing CuI (3809.0 mg, 20 mmol) at room temperature. The contents of the flask were then cooled to −78°C. The freshly prepared solution of alkylmagnesium bromide in THF (54 mL, 20 mmol) was then added dropwise with stirring at this temperature and stirred for 10 min. A solution of exo-methylene lactone (438.6 mg, 1.0 mmol) in THF (10 mL) was added very slowly, dropwise over 1.5 hr with vigorous stirring. The mixture was stirred at −78°C for 0.5 hr, after which time the reaction mixture was poured directly onto a plug of silica gel, packed in EtOAc, and eluted with EtOAc until product was no longer visible by TLC analysis. The filtrate was concentrated under reduced pressure. The residue was then purified by Si Gel flash column chromatography.

Procedure H: TBDPS deprotection

To a solution of *tert*-butyldiphenylsilyl protected alcohol (1.0 mmol) in THF (8 mL) was added a tetrabutylammonium fluoride (1.0 M in THF, 1.5 mL, 1.5 mmol). The resultant solution was heated to reflux and stirred for 48 hr. The reaction mixture was cooled to room temperature, EtOAc (10 mL) and saturated aq. NH_4Cl were added. The mixture was extracted with EtOAc (3 × 20 mL). The combined organic phase was dried over $MgSO_4$ and evaporated under vacuum. The residue was then purified by Si Gel flash column chromatography.

Procedure I: oxidation of alcohol

Dess-Martin periodinane (593.8 mg, 1.4 mmol) was added to a solution of alcohol (1.0 mmol) in CH_2Cl_2 (45 mL). The reaction mixture was stirred for 3 hr at rt, after which time it was concentrated to a few mL, re-dissolved in EtOAc (78 mL) and 78 mL of a 1:1 mixture of sat. aq. $NaHCO_3$: 10% aq. $Na_2S_2O_3$ was added. The organic extract was washed with H_2O (30 mL) and brine (30 mL). The aqueous extracts were then back extracted with EtOAc (3 × 40 mL) and all the organic extracts were combined and washed with H_2O (15 mL) and brine (8 mL). The organic extract was dried ($MgSO_4$), filtered and concentrated under reduced pressure. The residue was then purified by Si Gel flash column chromatography.

Procedure J: reductive amination

Ammonium acetate (770.8 mg, 10 mmol) was added to a solution of ketone (1.0 mmol) in anhydrous methanol (42.5 mL) at 30°C. Sodium cyanoborohydride (62.8 mg, 1.0 mmol) was added and the reaction mixture stirred for 12 hr at 30°C. The reaction mixture was quenched with aq. 10% HCl until pH 2. The mixture was concentrated under reduced pressure. The residue was dissolved in CH_2Cl_2 (10 mL) and H_2O (5 mL) and aqueous 5N NaOH was then added to ≈ pH 10 and stirred for 4 hr at rt. The organic layer was separated and the aqueous layer extracted with CH_2Cl_2 (3 × 50 mL). The combined organic extracts were dried (MgSO4), filtered and concentrated under reduced pressure. The residue was then purified by Si Gel flash column chromatography.

Procedure K: reductive amination

Benzylamine (131 μL, 128.6 mg, 1.2 mmol) was added to a solution of ketone (1.0 mmol) in anhydrous 1,2-dichloroethane (44 mL) at room temperature. The reaction mixture was stirred for 2 hr at room temperature. Glacial acetic acid (57.2 μL, 1.0 mmol) was added and stirred for a further 2 hr at rt. Sodium triacetoxyborohydride (211.9 mg, 1.0 mmol) was added in two portions, 0.50 mmol was added first and the reaction mixture stirred for 5 hr at rt, then 0.50 mmol was added and the mixture stirred for a further 24 hr at rt. The reaction mixture was quenched with saturated aqueous $NaHCO_3$ (50 mL), and extracted with EtOAc (3 × 50 mL). The

combined organic extracts were dried ($MgSO_4$), filtered and concentrated under reduced pressure. The residue was purified by Si Gel flash column chromatography.

Characterization of synthetic clionamines

Clionamine B (2): (Forestieiri et al., 2013). yellow wax; Rf: 0.03 (100% ethyl acetate); ^{1}H NMR (600 MHz, DMSO-d_6): δ 4.99–4.92 (1H, m), 3.11–3.01 (1H, m), 2.18–2.09 (1H, m), 2.07–2.02 (1H, m), 1.83–1.76 (1H, m), 1.76–1.69 (1H, m), 1.68–1.56 (3H, m), 1.56–1.37 (6H, m), 1.37–1.30 (2H, m), 1.30–1.25 (2H, m),1.25–1.02 (10H, m), 0.94–0.79 (8H, m), 0.76–0.70 (1H, m), 0.72 (3H, s), 0.68 (3H, s), 0.69–0.59 (1H, m). ^{13}C NMR (150 MHz, DMSO-d_6): δ 177.4, 82.0, 75.7, 61.2, 45.1, 40.1, 38.9, 38.1, 38.1, 35.9, 34.0, 31.6, 31.4, 31.1, 28.1, 27.5, 22.8, 22.3, 22.3, 20.9, 19.6, 13.4, 11.2. LRMS (ESI+): 432.3 $[M+H]^+$; HRMS (ESI+): $[M+H]^+$ 432.3478 calculated for $C_{27}H_{46}O_3N$; found 432.3475.

Compound 2.5.4 (5): white solid; Rf: 0.24 (60% EtOAc/hexanes); ^{1}H NMR (600 MHz, DMSO-d_6): δ 7.36 – 7.30 (4 H, m), 7.25 – 7.22 (1 H, m), 5.07 (1 H, m), 3.77 (1 H, br. s), 2.89 (1 H, br. s), 2.21 (1 H, m), 2.09 (1 H, m), 1.96 – 1.90 (1 H, m), 1.84 – 1.79 (1 H, m), 1.75 – 1.69 (2 H, m), 1.69 – 1.46 (7 H, m), 1.46 – 1.32 (5 H, m), 1.32 – 1.16 (9 H, m), 1.14 – 1.07 (2 H, m), 0.98 – 0.92 (1 H, m), 0.90 (3 H, d, J = 4.3), 0.89 (3 H, d, J = 4.3), 0.86 – 0.83 (1 H, m), 0.80 (3 H, s), 0.79 (3 H, s); ^{13}C NMR (150 MHz, DMSO-d_6): δ 177.8, 141.1, 128.5, 128.4 (2C), 128.2, 126.9, 83.1, 77.5, 61.5, 56.0, 53.9, 51.4, 51.2, 40.5, 39.4, 39.3, 38.3, 36.2, 34.5, 32.6, 32.2, 31.9, 31.8, 31.4, 29.7, 28.4, 27.9, 22.7, 22.4, 21.1, 20.0, 13.8, 11.6; LRMS (ESI+): 522.4 $[M + H]^+$; HRMS (ESI+): $[M+H]^+$ 522.3947 calculated for $C_{34}H_{52}O_3N$; found 522.3951.

Compound 2.3.4 (6): white solid, Rf: 0.31 (60% EtOAc/hexanes); ^{1}H NMR (600 MHz, $CDCl_3$): δ 7.37 – 7.29 (4 H, m), 7.27 – 7.21 (1 H, m), 4.77 – 4.72 (1 H, m), 3.78 – 3.70 (2 H, m), 2.94 – 2.92 (1 H, m), 2.66 – 2.60 (1 H, m), 2.28 – 2.24 (1 H, m), 2.24 – 2.17 (1 H, m), 1.97 – 1.83 (4 H, m), 1.71 – 1.58 (3 H, m), 1.58 – 1.34 (9 H, m), 1.34 – 1.04 (10 H, m). 0.95 (3 H, s), 0.89 (3 H, s), 0.88 (3 H, s), 0.82 (3 H, s). ^{13}C NMR (150 MHz, $CDCl_3$): δ 179.1, 141.0, 128.3 (2C), 128.1 (2C), 126.8, 82.7, 55.7, 54.7, 51.8, 51.3, 44.1, 42.3, 39.9, 39.3, 38.9, 36.8, 35.3, 34.9, 32.5, 31.1, 30.4, 29.7, 27.8, 26.9, 26.7, 26.4, 25.8, 24.0, 22.6, 22.6, 20.2, 13.8. LRMS (ESI+): 506.3 $[M+H]^+$; HRMS (ESI+): $[M+H]^+$ 506.3998 calculated for $C_{34}H_{52}O_2N$; found 506.3999.

Compound 2.3.6 (7): white solid; Rf: 0.32 (60% EtOAc/hexanes). ^{1}H NMR (600 MHz, $CDCl_3$): δ 7.35 – 7.29 (4 H, m), 7.25 – 7.21 (1 H, m), 4.93 (1 H, m), 3.78 – 3.70 (2 H, m), 2.95 (1 H, br. s), 2.57 (1H, m), 2.25 (1 H, m), 1.94 – 1.87 (2 H, m), 1.86 (1 H, d, J = 7.6), 1.79 – 1.73 (1 H, m), 1.72 – 1.66 (1 H, m), 1.52 (2 H, m), 1.51 – 1.40 (6 H, m), 1.35 (1 H, m), 1.33 – 1.29 (4 H, m), 1.29 – 1.23 (1 H, m), 1.19 – 1.15 (1 H, m), 1.15 – 1.05 (3 H, m), 0.96 (3 H, s), 0.73 (3 H, s). ^{13}C NMR (150 MHz, $CDCl_3$): δ 181.4, 141.0, 128.3 (2C), 128.1 (2C), 126.7, 82.9, 59.1, 54.7, 51.8, 51.3, 41.8, 40.1, 38.6, 36.7, 36.0, 35.3, 35.1, 33.0, 31.1, 30.4, 26.7, 26.5, 24.8, 23.9, 20.3, 18.0, 13.8. LRMS (ESI+): 436.5 $[M+H]^+$; HRMS (ESI+): $[M+H]^+$ 436.3216 calculated for $C_{29}H_{42}O_2N$; found 436.3221.

Compound 2.5.1 (8): white solid; Rf: 0.29 (60% EtOAc/hexanes); ^{1}H NMR (600 MHz, $CDCl_3$): δ 7.35 – 7.29 (4 H, m), 7.25 – 7.21 (1 H, m), 4.93 (1 H, m), 3.78 – 3.71 (2 H, m), 2.90 – 2.86 (1 H, m), 2.56 (1 H, m), 2.25 (1 H, m), 1.85 (1 H, m), 1.76 – 1.72 (1 H, m), 1.69 – 1.64 (1 H, m), 1.62 – 1.59 (1 H, m), 1.58 – 1.54 (1 H, m), 1.53 – 1.38 (6 H, m), 1.35 – 1.27 (2 H, m), 1.30 (3 H, m), 1.27 – 1.22 (2 H, m), 1.22 – 1.16 (2 H, m), 1.10 – 1.01 (2 H, m), 0.98 – 0.89 (1 H, m), 0.81 – 0.75 (1 H, m), 0.80 (3 H, s), 0.73 (3 H, s); ^{13}C NMR (150 MHz, CDCl3): δ 181.4, 141.1, 128.3 (2 C), 128.0 (2 C), 126.7, 82.8, 59.0, 54.7, 54.4, 51.4 (2 C), 41.7, 39.5, 38.3, 36.3, 36.0, 34.8, 33.3, 32.9, 32.6, 32.1, 28.4, 25.9, 20.0, 17.9, 13.8, 11.5; LRMS (ESI+): 436.5 $[M+H]^+$; HRMS (ESI+): $[M+H]^+$ 436.3216 calculated for $C_{29}H_{42}O_2N$; found 436.3219.

Compound 2.5.6 (9): white solid; Rf: 0.68 (neat EtOAc); ^{1}H NMR (600 MHz, $CDCl_3$): δ 4.75 (1 H, m), 3.62 – 3.55 (1 H, m), 2.62 (1 H, m), 2.28 – 2.18 (2 H, m), 1.97 – 1.89 (1 H, m), 1.87 – 1.83 (1 H, m), 1.83 – 1.78 (1 H, m), 1.73 – 1.65 (2 H, m), 1.65 – 1.60 (1 H, m), 1.60 – 1.52 (4 H, m), 1.52 – 1.31 (6 H, m), 1.31 – 1.28 (2 H, m), 1.28 – 1.21 (2 H, m), 1.21 – 1.15 (2 H, m), 1.13 – 1.09 (1 H, m), 1.07 (1 H, m), 0.96 (1 H, m), 0.88 (6 H, m), 0.82 (3 H, s), 0.82 (3 H, s), 0.68 – 0.62 (1 H, m); ^{13}C NMR (150 MHz, CDCl3): δ 179.0, 82.6, 71.2, 55.5, 54.6, 54.1, 44.7, 44.0, 42.2, 39.0, 38.9, 38.1, 36.9, 35.5, 34.6, 32.4, 32.0, 31.4, 28.4, 27.8, 26.9, 25.8, 22.6, 22.5, 20.4, 13.8, 12.3; LRMS (ESI+): 416.4 $[M+H]^+$; HRMS (ESI+): $[M+H]^+$ 416.3529 calculated for $C_{27}H_{46}O_2N$; found 416.3529.

Compound 2.5.5 (10): yellow wax; Rf: 0.29 (60% EtOAc/hexanes); ^{1}H NMR (600 MHz, $CDCl_3$): δ 7.38 – 7.28 (4 H, m), 7.27 – 7.21 (1 H, m), 4.74 (1 H, m), 3.77 (1 H, br. s), 2.89 (1 H, br. s), 2.62 (1 H, m), 2.29 – 2.23 (1 H, m), 2.23 – 2.16 (1 H, m), 1.97 – 1.89 (1 H, m), 1.87 – 1.81 (1 H, m), 1.70 – 1.38 (14 H, m), 1.38 – 1.14 (9 H, m), 1.10 – 1.03 (1 H, m), 0.97 – 0.90 (1 H, m), 0.88 (6 H, m), 0.85 – 0.75 (1 H, m), 0.81 (3 H, s), 0.79 (3 H, s); ^{13}C NMR (150 MHz, $CDCl_3$): δ 179.1, 141.1, 128.3 (3C), 128.1, 126.8, 82.6, 55.6, 54.6, 54.1, 51.4, 51.3, 44.0, 42.2, 39.5, 39.1, 38.9, 36.3, 34.6, 32.6, 32.4, 32.0, 29.7, 28.4, 27.8, 26.9, 25.8, 22.6, 22.5, 20.0, 13.8, 11.6; LRMS (ESI+): 506.5 $[M+H]^+$; HRMS (ESI+): $[M+H]^+$ 506.3998 calculated for $C_{34}H_{52}O_2N$; found 506.3991.

Compound 2.7.5 (11): yellow wax; Rf: 0.25 (neat EtOAc); ^{1}H NMR (600 MHz, DMSO-d_6): δ 7.48 – 7.42 (1H, m), 7.36 – 7.26 (3H, m), 7.23 – 7.17 (1H, m), 5.13 – 5.06 (1H, m), 4.92 – 4.84 (1H, m), 3.73 – 3.60 (1H, m), 2.78 – 2.71 (1H, m), 2.47 – 2.41 (1H, m), 2.22 – 2.14 (1H, m), 2.03 – 1.92 (3H, m), 1.74 – 1.60 (2H, m), 1.65 (3H, s), 1.60 – 1.53 (3H, m), 1.56 (3H, s), 1.53 – 1.41 (5H, m), 1.41 – 1.25 (7H, m), 1.25 – 1.02 (6H, m), 0.95 – 0.78 (2H, m), 0.78 – 0.71 (1H, m), 0.76 (3H, s), 0.69 – 0.59 (1H, m), 0.64 (3H, s); ^{13}C NMR (150 MHz, DMSO-d_6): δ 179.9, 131.2, 128.0, 127.9, 124.0, 82.4, 55.8, 53.9, 53.8, 50.5, 41.2, 40.6, 38.8, 37.5, 35.9, 34.4, 32.6, 31.9, 30.9, 28.1, 27.2, 27.1, 25.5, 19.7, 17.6, 13.6, 11.4. LRMS (ESI+): 518.8 $[M+H]^+$; HRMS (ESI+): $[M+H]^+$ 518.3998 calculated for $C_{35}H_{52}O_2N$; found 518.3989.

Compound 2.10.1 (12): white solid; Rf: 0.27 (neat EtOAc); ^{1}H NMR (600 MHz, DMSO-d_6): δ 5.13 – 5.05 (1H, m), 4.92 – 4.85 (1H, m), 2.77 – 2.66 (1H, m), 2.47 – 2.40 (1H, m), 2.36 – 2.24 (2H, m), 2.23 – 2.13 (1H, m), 2.03 – 1.92 (3H, m), 1.80 – 1.71 (2H, m), 1.70 – 1.59 (10H, m), 1.59 – 1.54 (4H, m), 1.54 – 1.41 (7H, m), 1.41 – 1.30 (5H, m), 1.30 – 1.03 (14H, m), 0.94 – 0.79 (4H, m), 0.79 – 0.66 (1H, m), 0.75 (3H, s), 0.63 (3H, s); ^{13}C NMR (150 MHz, DMSO-d_6): δ 179.9, 131.2, 124.0, 82.4, 55.8, 53.8, 41.2, 40.6, 38.7, 37.5, 5.9, 34.4, 32.6, 31.9, 31.2, 31.1, 30.9, 27.1, 26.3, 25.6, 25.5, 17.6, 13.6, 11.4; LRMS (ESI+): 524.5 $[M+H]^+$; HRMS (ESI+): 524.4469 $[M+H]^+$ calculated for $C_{35}H_{58}O_2N$; found 524.4468.

Compound 2.9.4a (13): ^{1}H NMR (600 MHz, CD_2Cl_2): δ 7.35 – 7.25 (6H, m), 7.23 – 7.14 (4H, m), 4.89 – 4.84 (1H, m), 3.70 – 3.59 (2H, m), 2.76 – 2.69 (1H, m), 2.64 – 2.55 (2H, m), 2.49 – 2.45 (1H, m), 2.20 – 2.14 (1H, m), 1.98 – 1.94 (1H, m), 1.90 – 1.73 (1H, m), 1.71 – 1.58 (5H, m), 1.58 – 1.41 (6H, m), 1.37 –1.24 (5H, m), 1.24 – 1.02 (6H, m), 0.94 – 0.84 (1H, m), 0.79 – 0.69 (1H, m), 0.75 (3H, s), 0.64 (3H, s); ^{13}C NMR (150 MHz, CD_2Cl_2): δ 179.9, 141.8, 128.3, 128.0, 127.9, 126.3, 125.8, 82.5, 55.8, 53.9, 53.8, 50.8, 50.6, 41.2, 40.5, 38.8, 37.4, 35.9, 34.7, 34.4, 32.6, 32.2, 31.9, 30.8, 28.9, 28.2, 25.5, 19.7, 13.6, 11.4; LRMS (ESI+): 540.4 $[M+H]^+$; HRMS (ESI+): 540.3842 $[M+H]^+$ calculated for $C_{37}H_{50}O_2N$; found 540.3845.

Compound 2.9.9 (14): white solid; Rf: 0.05 (neat EtOAc); ^{1}H NMR (600 MHz, DMSO-d_6): δ 7.36 – 7.25 (6H, m), 7.23 – 7.15 (4H, m), 5.75 – 5.69 (1H, m), 4.98 – 4.92 (1H, m), 3.75 – 3.59 (2H, m), 3.45 – 3.21 (1H, m), 2.77 – 2.70 (1H, m), 2.68 – 2.55 (2H, m), 2.16 – 2.07 (1H, m), 2.03 – 1.91 (2H, m), 1.89 – 1.79 (1H, m), 1.65 – 1.36 (9H, m), 1.36 – 1.22 (6H, m), 1.22 – 0.97 (7H, m), 0.93 – 0.79 (1H, m), 0.78 – 0.65 (1H, m), 0.73 (3H, s), 0.61 (3H, s); ^{13}C NMR (150 MHz, DMSO-d_6): δ 177.3, 141.9, 128.4, 128.2, 128.1, 128.1, 128.0, 127.9, 127.9, 127.9, 126.4, 125.7, 82.0, 75.6, 61.2, 55.1, 53.4, 50.8, 50.6, 40.1, 39.9, 38.7, 38.0, 35.8, 35.5, 34.0, 32.8, 32.1, 31.6, 31.1, 30.6, 28.1, 25.5, 25.4, 19.6, 13.3, 11.4; LRMS (ESI+): 556.2 $[M+Na]^+$; HRMS (ESI+): 556.3791 $[M+H]^+$ calculated for $C_{37}H_{50}O_3N$; found 556.3782.

Compound 3.3.3 (15): yellow wax; Rf: 0.23 (60% EtOAc/hexanes); ^{1}H NMR (600 MHz, DMSO-d_6): δ 7.37 – 7.26 (4H, m), 7.24 – 7.18 (1H, m), 4.93 – 4.87 (1H, m), 3.74 – 3.60 (2H, m), 2.79 – 2.72 (1H, m), 2.69 – 2.64 (1H, m), 2.49 – 2.44 (1H, m), 2.22 – 2.15 (1H, m), 1.99 – 1.95 (1H, m), 1.72 – 1.67 (1H, m), 1.66 – 1.60 (2H, m), 1.60 – 1.39 (11H, m), 1.38 –1.25 (5H, m), 1.22 (3H, s), 1.21 – 1.18 (3H, m), 1.18 – 1.04 (5H, m), 0.95 – 0.83 (1H, m), 0.78–0.72 (1H, m), 0.76 (3H, s), 0.65 (3H, s). ^{13}C NMR (150 MHz, DMSO-d_6): δ 179.8, 141.3, 127.9, 126.4, 82.4, 62.9, 62.8, 57.5, 55.8, 55.8, 53.9, 53.8, 50.5, 41.2, 40.7, 40.5, 38.7, 37.4, 35.9, 34.4, 32.6, 32.1, 31.8, 31.0, 30.9, 28.1, 27.9, 27.8, 24.6, 24.0, 23.9, 19.6, 18.6, 13.5, 11.4. LRMS (ESI+): 534.3 $[M+H]^+$; HRMS (EI): 533.38689 $[M]^+$ calculated for $C_{35}H_{51}O_3N$; found 533.38751.

Compound 3.2.7 (16): yellow wax; Rf: 0.57 (10% MeOH/CH_2Cl_2); ^{1}H NMR (600 MHz, DMSO-d_6): δ 7.35 – 7.16 (5H, m), 4.92 – 4.85 (1H, m), 4.37 – 4.30 (1H, m), 4.07 – 4.03 (1H, m), 3.70 – 3.59 (2H, m), 3.10 – 3.03 (1H, m), 2.75 – 2.69 (1H, m), 2.65 – 2.60 (1H, m), 2.47 – 2.41 (1H, m), 2.23 – 2.15 (1H, m), 2.02 – 1.94 (1H, m), 1.73 – 1.66 (1H, m), 1.66 – 1.61 (1H, m), 1.60 – 1.42 (8H, m), 1.37 – 1.27 (5H, m), 1.27 – 1.05 (10H, m), 1.05 – 1.01 (2H, m), 1.00 – 0.94 (2H, m), 0.94 – 0.82 (2H, m), 0.82 – 0.69 (1H, m), 0.76 (3H, s), 0.64 (3H, s). ^{13}C NMR (150 MHz, DMSO-d_6): δ 180.1, 141.5, 129.7, 128.5, 82.4, 77.2, 76.9, 75.8, 71.6, 63.1, 55.7, 53.9, 41.2, 40.7, 37.5, 34.3, 33.7, 32.6, 31.7, 31.3, 30.5, 30.3, 29.0, 28.7, 26.4, 26.3, 24.5, 24.3, 22.1, 19.6, 13.9, 13.6, 11.3; LRMS (ESI+): 552.5 $[M+H]^+$; HRMS (ESI+): 552.4053 $[M+H]^+$ calculated for $C_{35}H_{53}O_4N$; found 552.4034.

Compound 3.3.5 (17): orange wax; Rf: 0.43 (10% MeOH/CH_2Cl_2); ^{1}H NMR (600 MHz, CH_2Cl_2): δ 7.48 – 7.43 (1H, m), 7.43 – 7.36 (1H, m), 7.36 – 7.31 (1H, m), 7.31 –7.25 (1H, m), 4.86 – 4.80 (1H, m), 4.15 – 4.07 (2H, m), 4.03 (1H, s), 3.48 – 3.38 (1H, m), 3.15–3.06 (1H, m), 2.49 – 2.39 (2H, m), 2.28 – 2.18 (1H, m), 1.97 – 1.90 (1H, m), 1.81 – 1.63 (6H, m), 1.63 – 1.38 (10H, m), 1.38 – 1.18 (6H, m), 1.18 – 1.14 (3H, m), 1.14 – 1.11 (3H, m), 1.08 –0.93 (3H, m), 0.86 – 0.81 (2H, m), 0.79 (3H, s), 0.71 (3H, s), 0.74 – 0.67 (1H, m). ^{13}C NMR (150 MHz, CH_2Cl_2): δ 180.9, 141.3, 129.7, 129.3, 128.9, 83.5, 83.5, 81.9, 79.6, 77.0, 76.8, 73.4, 57.2, 57.1, 54.8, 52.8, 50.5, 41.9, 41.9, 39.6, 38.6, 36.5, 35.2, 33.4, 32.3, 32.2, 31.2, 31.2, 28.5, 25.3, 25.1, 21.5, 20.5, 19.7, 14.3, 11.6; LRMS (ESI+): 590.5 $[M+H]^+$; HRMS (ESI+): 590.4209 $[M+H]^+$ calculated for $C_{38}H_{55}O_4N$; found 590.4211.

BIOCB (18): (see Scheme S1) ^{1}H NMR (600 MHz, DMSO-d_6): δ 8.04 – 7.95 (1H, m), 6.52 – 6.41 (2H, m), 5.78 – 5.69 (1H, m), 4.99 – 4.91 (1H, m), 4.32 – 4.27 (1H, m), 4.16 – 4.08 (1H, m), 3.73 – 3.68 (1H, m), 3.64 – 3.59 (1H, m), 3.39 – 3.33 (3H, m), 3.18 – 3.11 (3H, m), 2.93 – 2.89 (1H, m), 2.83 – 2.77 (1H, m), 2.60 – 2.54 (1H, m), 2.15 – 2.08 (1H, m), 2.08 – 2.00 (4H, m), 1.90 – 1.81 (1H, m), 1.81 – 1.73 (1H, m), 1.73 – 1.53 (7H, m) 1.53 – 1.36 (10H, m), 1.36 – 1.00 (15H, m), 0.92 – 0.80 (9H, m), 0.77 – 0.69 (3H, m), 0.65 (3H, s), 0.68 – 0.57 (1H, m). ^{13}C NMR (150 MHz, DMSO-d_6): δ 177.4, 172.3, 162.9, 82.0, 75.7, 69.8, 69.8, 69.8, 69.7, 69.7, 69.7, 69.6, 69.3, 69.1, 66.6, 65.8, 61.1, 59.3, 59.2, 55.9, 55.5, 55.0, 52.9, 44.1, 42.9, 38.5, 38.4, 38.1, 36.0, 35.4, 35.3, 35.2, 35.1, 33.9, 31.4, 31.4, 31.2, 28.3, 28.1, 27.5, 25.4, 22.8, 22.4, 21.0, 13.4, 11.8. LRMS (ESI+): 877.9 $[M+H]^+$; HRMS (ESI+): $[M+H]^+$ 877.5724 calculated for $C_{47}H_{81}O_9N_4S$; found 877.5734.

QUANTIFICATION AND STATISTICAL ANALYSIS

Autophagy Stimulation: Figures S1 and S2: Software - Microsoft Excel for Mac, data are means of replicate measurements of punctate flourescence, n = 3.

Mtb Infection and THP-1 Cytotoxicity, Figures 2, 3B, 3C, 5B, 5C, 6B, and 6C**:** Details regarding statistical tests and analysis for Mtb infection experiments, cell cytotoxicity due to compound treatment, and qPCR results can be found in their respective figure legends and the method details sections. Data are presented as the mean + or ± SEM of the indicated *n* where *n* is the number of replicate wells of 96-well plate(s), representative of two to four separate experiments. For all dose response curves, non-linear regression was used to fit the data of the log (inhibitor) vs. response (variable slope) curve using Graphpad Prism analysis software. Statistical analysis was performed using the indicated t tests using Graphpad Prism software.

Chemical Genetics, Figures 3D–3G, 6D–6G, S3, and S5: Chemical-genetic interactions were computed as z-scores representing the standard deviation of each strain in the condition profile with respect to its counterpart strain in the reference DMSO profile. Chemical-genetic interaction z-scores (CG z-scores) were calculated by comparing the profile of log read counts from each condition across all strains in a mutant collection to a reference profile of log read counts across all strains. The reference profile was calculated as the log of strain-wise average profiles across all DMSO (vehicle only control) read count profiles, excluding read counts less than 20 which were excluded from the calculation. The log read count profile for each condition was LOWESS normalized with respect to

the reference DMSO profile. A condition-specific standard deviation and a reference (DMSO) standard deviation vector was used to calculate z-scores. The condition-specific standard deviation was calculated on the middle 75% of strain-wise deviations between each condition profile and reference profile. The reference standard deviation vector was calculated using all DMSO control profiles (n>3 per screen), as the square root of the LOWESS-derived estimate (span = 30%) of the squared deviations with respect to the reference profile. Separate standard deviation vectors were computed for positive interactions and negative interactions, and the final reference standard deviation vector was specific to each individual condition depending on the signs of the deviations in that condition. Chemical genetic z-scores were then calculated as the deviation from the reference divided by the larger value among: 1) the condition-specific standard deviation, or 2) the positive or negative standard deviation from the reference S.D. vector. Since CG profiles do not follow a normal distribution, Tukey's method (Tukey, 1977) was used to determine extreme outliers in a profile based on the interquartile range of the distribution of CG z-scores. Profiles at concentrations that showed the best separation between outlier chemical genetic interactions and the mean z-score for all interactions in the profile were selected as the representative profiles for each mutant pool.

PIk1 Inhibition in the TGN, Figure 4D: Box and whisker plot showing the peak TGN fluorescence intensity after 1 hour of the indicated treatments. The boxes show the inter-quartile range (1st-3rd), the whiskers show the highest and lowest measurements excluding outliers, and the horizontal bar within each box shows the median. n = 53 represents the number of yeast cells sampled. Asterisks indicate p-value < 0.05 according to unpaired two-tailed student's t-tests. Software - ImageJ and Microsoft Excel.

MS/MS pulldown data, Figure 5A: Proteins that most strongly interact with biotinylated Clionamine B were determined by AP-MS from a wildtype *S. cerevisiae* strain (BIOCB (18), n=3, SAINT FDR $\leq$1%) as well as a strain that overproduced *PIK1* (BIOCB (18) - PIK1). The mean spectral count for each interacting protein was calculated. Samples that were loaded with biotinylated cholesterol and beads alone served as controls. To identify significant interaction partners from the affinity purification data, the data were subjected to Significance Analysis of INTeractome express (SAINTexpress 3.6.1) analysis (Teo et al., 2014) implemented in ProHits. To perform SAINTexpress analysis, samples generated with immobilized biotinylated compounds were compared to beads-only controls and to beads onto which cholesterol (instead of RP-3-161) was immobilized. Controls (seven) were compressed to four virtual controls in which the highest spectral counts value for each prey were kept to increase stringency in scoring. Each of the four biological replicate purifications from compound RP-3-161, including the purification exposed to lysate overexpressing PIK1, were analyzed with SAINT separately and the Averaged SAINTexpress value across the four replicates was used to calculate the Bayesian FDR (this ensures that only those hits that are confidently detected across all replicates are reported). Proteins with FDR below or equal to 1% were considered to be statistically significant. The clionamine B-PIK1 interaction is only observed using cell lysate extracted from a *PIK1* overproducing yeast strain, but is 7-fold stronger than the cholesterol-PIK1 interaction from the same overproducing strain (BIOCB (18)-PIK1, n =1; Cholesterol-PIK1, n =2)